Machine learning-constrained projection of bivariate hydrological drought magnitudes and socioeconomic risks over China

Rutong Liu[1], Jiabo Yin[1*], Louise Slater[2], Shengyu Kang[1], Yuanhang Yang[1], Pan Liu[1], Jiali Guo[3,4], Xihui Gu[5], Xiang Zhang[6], Aliaksandr Volchak[7]

[1]State Key Laboratory of Water Resources Engineering and Management, Wuhan University, Wuhan, Hubei, 430072, P.R. China

[2]School of Geography and the Environment, University of Oxford, Oxford, UK

[3]Engineering Research Center of Eco-environment in Three Gorges Reservoir Region, Ministry of Education, China Three Gorges University, Yichang, Hubei 443002, China

[4]College of Hydraulic and Environmental Engineering, China Three Gorges University, Yichang, Hubei 443002, China

[5]School of Environmental Studies, China University of Geosciences, Wuhan 430074, China

[6]National Engineering Research Center of Geographic Information System, School of Geography and Information Engineering, China University of Geosciences, Wuhan 430074, China

[7]Engineering Systems and Ecology Faculty, Brest State Technical University, Moskovskaya 267, 224017 Brest, Belarus

*Correspondence: Jiabo Yin (jboyn@whu.edu.cn)

Abstract

Climate change influences the water cycle and alters the spatiotemporal distribution of hydrological variables, thus complicating the projection of future streamflow and hydrological droughts. Although machine learning is increasingly employed for hydrological simulations, few studies have used it to project hydrological droughts, not to mention the bivariate risks, referring to drought duration and severity, as well as their socioeconomic effects under climate change. We developed a cascade modeling chain to project future bivariate hydrological drought characteristics in 179 catchments over China, using 5 bias-corrected GCM outputs under three shared socioeconomic pathways, five hydrological models and a deep learning model. We quantified the contribution of various meteorological variables to daily streamflow by using a random forest model, then employ terrestrial water storage anomalies and a standardized runoff index to evaluate recent changes in hydrologic drought. Subsequently, we constructed a bivariate framework to jointly model drought duration and severity by using Copula functions and the most likely realization method. Finally, we used this framework to project future risks of hydrological droughts as well as associated exposure of gross domestic product and population. Results showed that our hybrid hydrological-deep learning model achieved >0.8 Kling-Gupta efficiency in 161 out of 179 catchments. By the late 21st century, bivariate drought risk is projected to double over 60% of catchments mainly located in Southwest China under SSP5-85, which shows the increase of drought duration and severity. Our hybrid model also projected substantial GDP and population exposures by increasing bivariate drought risks, suggesting an urgent need to design climate mitigation strategies toward a sustainable development pathway.

1 Introduction

In a warming world, the change of the global water cycle is expected to alter the regional and seasonal distribution of key hydrological variables such as precipitation and evapotranspiration (Allan et al., 2020; Yin et al., 2023b). As precipitation patterns are particularly sensitive to changes in atmospheric forcing and local conditions, precipitation extremes are generally increasing globally, exacerbating spatial heterogeneity of precipitation (Donat et al., 2016; Tabari, 2020). A suite of Shared Socioeconomic Pathways (SSPs) has been proposed to simulate different possible future scenarios of social responses to climate change, and these are employed to investigate the possible effects of long-term climate change (Meinshausen et al., 2020; Zhang et al., 2021). By using the SSP framework, numerous works have indicated that the redistribution of precipitation may lead to the decline of water storage in some regions, and intensify water scarcity in arid regions (Sönmez and Kale, 2018; Woolway et al., 2020; Yao et al., 2023). Under increasing atmospheric greenhouse gases, numerous studies have reported a widespread increase in drought events, even in areas with increasing annual runoff (Dai et al., 2018). The rapidly changing distribution of precipitation and other meteorological elements under climate change complicates projection of future runoff and drought.

China's socioeconomic development, particularly its agricultural sector, is threatened by the rapid intensification of extreme hazards under climate change (Piao et al., 2010). Over the past years, China has been hit by severe drought events which have caused considerable damage to ecosystem productivity and socio-economic growth (Yin et al., 2023; Zhai and Zou, 2005). For instance, one extreme drought in Sichuan Province in 2022 resulted in power shortages and led to economic losses of 669 million dollars. Water shortage is also a key challenge that hinders the sustainable development of the North China Plain (Chen and Yang, 2013). Over the period of 1985-2014, drought accounted for about 19% of economic losses among all meteorological hazards (Chen and Sun, 2019). With continuing global warming, the economic losses from severe drought events might increase by over ten billion US dollars per year by the late 21st century, underscoring the importance of projecting future droughts over China (Lu et al., 2023).

Droughts can be triggered by divergent mechanisms, and are thus distinguished according to the type of drought, such as meteorological and hydrological drought (Yihdego et al., 2019). The majority of studies have focused on meteorological droughts, which can then be translated to a hydrological drought, while fewer works have focused on hydrological drought probably due to a lack of measurements like the standardized runoff index (SRI) (Barker et al., 2016; Kumar et al., 2016; Tirivarombo et al., 2018). Furthermore, hydrological droughts are not only affected by the water cycle but also by human interventions, which makes them difficult to accurately be predicted (Wu et al., 2021). Currently, the majority of drought impact assessments focus on the investigation of individual drought variables (i.e., drought duration, severity, intensity, etc.) through univariate probabilistic models and stochastic theory (Byakatonda et al., 2018; Myronidis et al., 2018; Zhang et al., 2022). However, univariate drought analysis cannot accurately describe the probability of drought events, because droughts of either long duration or severe intensity can lead to substantial socio-ecosystem damages (Castle et al., 2014; Udall and Overpeck, 2017). Therefore, the bivariate framework based on Copula functions has been developed for drought projection, compensating for the incompleteness of a single variable analysis (Ayantobo et al., 2017; Nabaei et al., 2019). At present, studies on hydrological drought within a bivariate framework are still lacking. Beyond the choice of approach (univariate or bivariate), the Gravity Recovery and Climate Experiment (GRACE) and GRACE-FO (GRACE Follow-On) satellites now provide two decades of large-scale terrestrial water storage (TWS) data, which captures the water deficit in various forms on land and can be used to monitor droughts (Schmidt et al., 2006). The drought severity index based on TWS (TWS-DSI) can be used to monitor past drought events, which also shows potential advantages in drought warning, forecasting, and projection (Nie et al., 2018; Pokhrel et al., 2021).

In recent decades, many studies have used bias-corrected outputs from Global Climate Models (GCMs) to project future hydrological drought scenarios (e.g., (Ashrafi et al., 2020; Dixit et al., 2022; Kim et al., 2021). The growing application of machine learning has revealed a high potential for improving the accuracy of hydrological simulation and prediction (Mokhtar et al., 2021). In recent years, many machine learning algorithms have been adopted in drought simulation and produce good performance, such as wavelet neural networks (WNNs) (Xiujia et al., 2022), support vector machines (SVMs) (Zhu et al., 2021) and long short-term memory neural networks (LSTMs) (Dikshit et al., 2021a)). These algorithms can be used to simulate the evolution of future droughts and construct risk maps for drought contingency planning (Rahmati et al., 2020). Among the different models, the LSTMs can effectively simulate short-term and long-term streamflow series, and their performances have been validated at short temporal scales (Dikshit et al., 2021b; Kang et al., 2023).

In this study, we projected changes in bivariate hydrological drought characteristics (duration and severity) and their associated socioeconomic risks under three SSPs (i.e., SSP1-26, SSP3-70, and SSP5-85) over 179 catchments in China. To achieve this, we combined five hydrological models and a deep learning model (i.e., the LSTM), and then drove the hybrid models with the five bias-corrected GCMs outputs under the Coupled Model Intercomparison Project phase six (CMIP6). Then, we employed a machine learning-based framework (i.e., Random Forest, RF model) to quantify the sensitivity of daily streamflow to different meteorological variables. We employed the run theory and two drought metrics, the SRI and TWS-DSI, to identify and explore recent changes in drought characteristics. In addition, we used Copula functions to build the bivariate model of drought duration and severity during both reference and future periods. After identifying shifts in bivariate drought characteristics based on the most likely realization approach, we projected the exposure of gross domestic product (GDP) and population to increasing drought risks in the future. Finally, we decomposed the uncertainties arising from different sources by employing the multivariate analysis of variance (MANOVA) method. This study illustrated the used materials and methods in Section 2 and Section 3, respectively. We compared SRI and TWS-DSI in assessing drought conditions in Section 4.1. The contribution of meteorological factors to simulate streamflow and the calibration of hybrid terrestrial models were shown in Section 4.2. The evolution of univariate droughts was projected in Section 4.3. The bivariate droughts of future scenarios and associated socioeconomic exposures were evaluated in Section 4.4. We discussed the uncertainty of our analysis and main limitations of this study in Section 5, and finally summarized our work in Section 6.

2. Methodology

The workflow of this study is divided into four modules (Figure 1), described briefly below and detailed in the following sections. In step 1, the hydrological models and LSTM are trained using the ERA5-Land dataset, and then the output of HMs is used as input to feed the LSTM, thus we build the hybrid terrestrial models (HTMs). In step 2, the trained HTMs are validated using in situ streamflow observations, then driven by using the outputs of five GCMs from the CMIP6 to project streamflow and the SRI series. In step 3, monthly drought characteristics (i.e., drought duration and severity) are defined using run theory and combined with Copula functions to construct a bivariate drought framework. Future bivariate drought change is evaluated using the most likely realization method. Meanwhile, the TWS measurements from GRACE missions are also employed to characterize recent changes in TWS-based droughts, which are also compared with the hydrological droughts. In step 4, we employ future scenarios of GDP and population alongside our future drought projections to produce a socioeconomic assessment of drought exposure over China. Finally, we examine the contribution of uncertainty from different sources in projecting drought change and exposure.

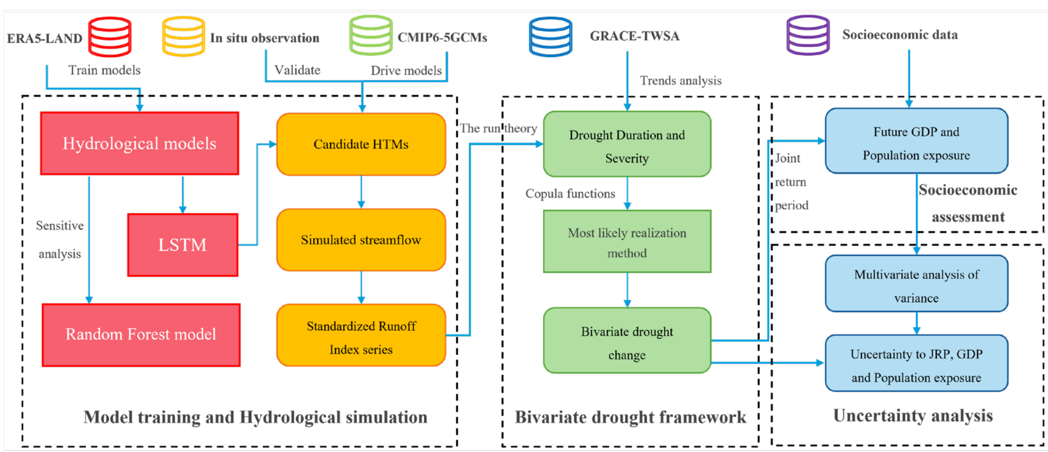

Figure 1. Schematic flowchart of the method, including ML-constrained hydrological simulations, evaluation of bivariate hydrologic drought characteristics and change, and the socioeconomic evaluation to drought exposure under climate change.

2.1 Derivation of 2-meter relative and specific humidity

As relative humidity and specific humidity are not directly available from the ERA5-land dataset, we estimate these two variables based on the physical relationship in atmosphere. The Clausius–Clapeyron relationship is used to derive saturated vapor pressure (e_s) and air temperature (T), and is expressed as follows (Koutsoyiannis, 2012):

$$e_s(T) = e_0 \exp\left[(\frac{1}{T_0} - \frac{1}{T}) \frac{L_0}{R_0} \right] \tag{1}$$

where T_0, e_0, L_0 and R_0 are freezing temperature in Kelvin, saturated vapor pressure under freezing temperature, latent heat of vaporization and gas constant of water vapor, with a value of 273.15 K, 611 Pa, 2.5×10^6 J kg^{-1}, 461 J kg^{-1} K^{-1}, respectively;

Since near-surface relative humidity (*RH*) can't be directly obtained from the ERA5-Land dataset, the 2m temperature (T_{2m}) and dew-point temperature (T_d) are substituted into equation (1) to calculate *RH*:

$$RH = \frac{e_s(T_d)}{e_s(T_{2m})} = \exp\left[(\frac{1}{T_{2m}} - \frac{1}{T_d}) \frac{L_0}{R_0} \right] \tag{2}$$

Then, the near-surface air pressure (*ps*) and T_d are used to deduce the specific humidity (*SH*), which is mathematically expressed as follows (Simmons et al., 1999):

$$SH = \frac{0.622 \times e_s(T_d)}{ps - 0.378 e_s(T_d)} \tag{3}$$

2.2 Sensitivity analysis on meteorological variables for runoff

The RF model (Catani et al., 2013) is used to calculate the sensitivity of runoff to different meteorological variables, including precipitation (*pr*), air pressure (*ps*), surface downwelling shortwave and longwave radiation (*srsds and srlds*), *RH*, *SH,* average temperature, maximum and minimum temperature. The contribution of a key variable is derived by using the pre-established model, the perturbed meteorological variable and remaining (non-perturbed) variables (Antoniadis et al., 2021; Green et al., 2020). The percentage change in streamflow is derived from the following equation:

$$S_i = \frac{\text{mean}\left(R_{(i+1\text{SD})} - R_{(all)}\right)}{\text{stdev}\left(R_{obs}\right)} \times 100\% \tag{4}$$

where S_i indicates the sensitivity of streamflow to i^{th} meteorological variable, which are *pr*, *ps*, *SH*, *RH*, *srlds*, *srsds* and temperature; R_{obs} is the observation of streamflow which has units of m^3/s; $R_{(i+1SD)}$ is the simulated streamflow by perturbing *i* by +1 SD; $R_{(all)}$ is the streamflow simulated by all meteorological variables; stdev (R_{obs}) represents the standard deviation of $R_{obs.}$

2.3 Deep learning-constrained hydrological modeling

2.3.1 Conceptual hydrological models

For preliminary hydrological simulations, we select five hydrological models to represent hydrological characteristics under different environments. The GR4J (Génie Rural à 4 paramètres Journalier) is a lumped model with 4 parameters developed by Perrin et al. (2003). GR4J consists of two water store modules (runoff yielding and routing) and uses daily rainfall and evapotranspiration as inputs to simulate streamflow series (Kunnath-Poovakka and Eldho, 2019). This model has been successfully used to simulate hybrid runoff processes on many continents (Gu et al., 2023; Shin and Kim, 2021). Additionally, we use the temperature-based method (Oudin et al., 2005) to estimate the potential evapotranspiration of the GR4J model.

The HBV (Hydrologiska Byråns Vattenbalansavdelning) model was initially developed by the Swedish Meteorological and Hydrological Institute for Hydrological Forecasting (BERGSTRÖM and FORSMAN, 1973). This model includes five modules and one transform function to quantify hydrological variables (i.e., precipitation, snow, soil moisture, runoff, baseflow) (Bergström, 1995). It has been widely employed to simulate streamflow, and it particularly has a good capacity for simulating snowmelt runoff (Kriauciuniene et al., 2013).

The HMETS (hydrological model of École de technologie supérieure) model contains 21 parameters and two reservoirs (i.e., the saturated and vadose zones), which is considered to efficiently complete hydrological simulation in limited scales (Martel et al., 2017). The model can simulate six processes in water cycle, including the accumulation, melts and refreezing of snow, water infiltration and routing, and evapotranspiration (Qi et al., 2020). It has been growly used for streamflow simulation under climate change and has shown great performance (Chen et al., 2018).

The SIMHYD (simple lumped conceptual daily rainfall-runoff) model is a daily rainfall-runoff model developed by Porter and McMahon (1975). There are four types of water fluxes from different sources: impervious areas, infiltration, interflow, and groundwater storage (Chiew et al., 2002). Although the model was developed earlier, it has shown good accuracy in simulating runoff over China (Yu and Zhu, 2015).

The XAJ (Xinanjiang) model is a hydrological model, which can usually achieve better performance in humid and semi-humid areas than in arid areas (Ren-Jun, 1992). As the model was developed based on the underlying surface of the Yangtze River Basin in China, it is composed of a three-layer evapotranspiration module with four parameters and separates the runoff into four components (i.e., surface water, groundwater, interflow water and flow routing) (Tian et al., 2013). To date, it is widely reported that the XAJ model usually shows a great performance in simulating hydrological conditions in China (Hu et al., 2005; Jiang et al., 2007). However, due to inadequacies in the simulation of arid regions, the results of the XAJ model did not be considered as the best option in northern China.

We used the SCE-UA (Shuffled Complex Evolution) approach to maximize the objective function (i.e., Kling-Gupta efficiency) to optimize these models (Duan et al., 1992). The most complete 20-year observation period is selected to calibrate five models in each watershed by a daily time step. To calibrate the hydrological models, a cross-validation method developed by Arsenault et al. (2017) is used for calibration, which employs the odd years of data to calibrate models, and the even years of data to validate. As catchments are located in different climatic regions, the parameters of models are calibrated for each catchment, which means that the parameters are not universal. Although uncertainties shown by hydrological models are ineradicable, the overall uncertainty is acceptable in the current scale after optimizing five hydrological models for each catchment.

2.3.2 Hybrid scheme of hydrological model and machine learning

Recurrent neural network (RNN) models have had considerable success in hydrological modeling (Cho et al., 2014; Sherstinsky, 2020). However, when considering long input sequences, RNNs struggle to capture the relationships between distant points due to a phenomenon known as "long-term dependencies" (Yu et al., 2019). With the development of deep learning, this problem can be successfully avoided by using LSTMs.

An LSTM cell includes input, output and forget gates. The input gate determines which new information can be stored in the cell state, and the forget gate identifies which information will be discarded from the cell state. The output gate controls what part of the cell state is selected as the output. The updated cell state is a combination of the information retailed and the new information to be added. By using this architecture, the LSTM can avoid the problem of gradient vanishing or explosion during backpropagation, especially when a series is long (Gers et al., 2000). The LSTM can be expressed as follows:

$$fg_t = \sigma(W_{hf} hs_{t-1} + W_{xf} x_t + b_f) \quad (5)$$

$$ig_t = \sigma(W_{hi} hs_{t-1} + W_{xi} x_t + b_{fg}) \quad (6)$$

$$\tilde{c}_t = \tanh(W_{h\tilde{c}} hs_{t-1} + W_{x\tilde{c}} x_t + b_{\tilde{c}}) \quad (7)$$

$$c_t = fg_t \cdot c_{t-1} + ig_t \cdot \tilde{c}_t \quad (8)$$

$$og_t = \sigma(W_{ho} hs_{t-1} + W_{xo} x_t + b_o) \quad (9)$$

$$hs_t = og_t \odot \tanh(c_t) \quad (10)$$

where x_t, fg_t, ig_t and og_t are input variables, and forget, input and output gates at time *t*, respectively; $W.$ are the weights, where W_i, $W_{\tilde{c}}$, W_f and W_o are the weights of each gate, $W_{x\cdot}$ are the weights of each gate at time t, $W_{h\cdot}$ are the weights of each gate at the former time $t-1$; the operator '$\odot$' is the symbol for the dot product of two vectors; c_t and hs_t are the cell state of the LSTM and the hidden unit at time t, respectively; c_{t-1} and hs_{t-1} at the former time $t-1$; $\tilde{c}_t$ is the activation function of hidden layer; b_i, b_f, b_o and b_c are bias itemsand the; σ (·) and tanh (·) are the sigmoid function and the hyperbolic tangent function, respectively; at the initial moment, cell and hidden states are set to zero arrays.

The hydrological outputs together with other climate variables are used as inputs to feed the LSTM model (i.e., the LSTM is thus constrained by the HMs). Because changes in meteorological variables require some time to converge before they are reflected in the runoff, it is essential to calculate the lag time caused by the flow convergence for the model. The catchment response lag time *d* is defined as the time during which precipitation accumulates in the river to generate runoff for the gauge downstream, and is mathematically expressed as follows (Berne et al., 2004; Ganguli and Merz, 2019):

$$d = 2.51 A_d^{0.4} [\text{ hrs }] = 0.11 A_d^{0.4} [\text{ days }] \tag{11}$$

where A_d (km^2) represents the catchment area; meteorological variables from day *T*-d to day *T* are employed to drive HTMs.

We combine the five hydrological models with LSTM to construct five HTMs. To compare the performance of the HTMs, we use ten HTMs as candidates for streamflow simulation in each catchment. The calibrated HTMs are then driven by the outputs of five GCMs under each SSP (aggregated to produce a basin average series) during 1985-2100 over 179 catchments to project future daily streamflow.

2.4 Drought indexes and run theory

The TWS-DSI is employed to measure the degree of terrestrial drought severity (Zhao et al., 2017). It is a dimensionless standardized water storage anomaly index, which can indicate terrestrial drought conditions when below the mean standard value. The TWS-DSI can be mathematically expressed as follows:

$$TWS\text{-}DSI_{x,y} = (TWS_{x,y} - \overline{TWS_y}) / \sigma_y \tag{12}$$

where $TWS_{x,y}$ is the TWS at year *x* and month *y*; $\overline{TWS_y}$ and σ_y represent the means and standard deviation of TWS at month *y*, respectively.

The SRI is a measure of the variability of runoff for a given duration based on the percentage of accumulated runoff. (Shukla and Wood, 2008). The hydrological drought classification and ranges indicated by SRI are shown in Table S1. To calculate the SRI, we simulate the retrospective time series of streamflow and fit the sample series to a probability distribution. The SRI is considered to follow a Pearson type-III distribution (Vicente-Serrano et al., 2012), and is calculated as follows:

$$SRI = \begin{cases} -(r - \dfrac{c_0 + c_1 r + c_2 r^2}{1 + d_1 r + d_2 r^2 + d_3 r^3}) & 0 < F(x) \le 0.5 \\ r - \dfrac{c_0 + c_1 r + c_2 r^2}{1 + d_1 r + d_2 r^2 + d_3 r^3} & 0.5 < F(x) \le 1 \end{cases} \tag{13}$$

where $r = \sqrt{\ln\left[\dfrac{1}{F(x)^2}\right]}$; $F(x)$ is the cumulative probability density of SRI; c_0, c_1, c_2, d_1, d_2 and d_3 are the empirical constants, taken as 2.516, 0.803, 0.010, 1.433, 0.189, 0.001, separately.

After calculating the two drought indexes, the degree of water deficit can be determined according to the Grades of Meteorological Drought and the previous classification (Dikici, 2020). Table S1 presents the drought classification and thresholds used for identifying drought degrees. The run theory is employed to obtain characteristics of drought events from the time series (Yevjevich, 1967). When the drought index is below the mild drought (i.e., ≤-0.5 drought index), a drought event is detected (Figure 2), and then the drought duration and drought severity are extracted.

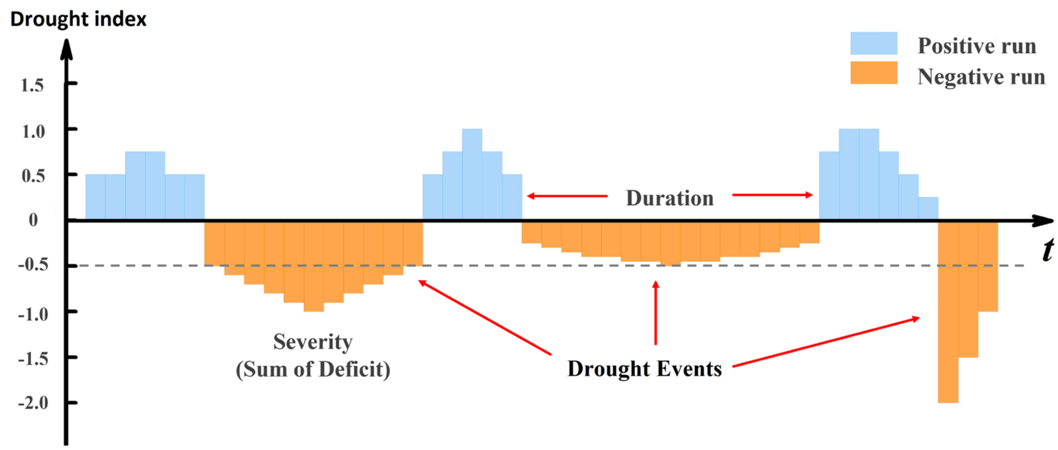

Figure 2. Drought duration and severity identification based on run theory, where -0.5 denotes the drought threshold (grey dash line).

2.5 Socioeconomic exposure assessments based on the Copulas and most likely realization

To integrate the assessment of drought change arising from the duration and severity under climate change, we employed a Copula framework by constructing joint probability distribution of two variables. After extracting the drought duration (*D*) and severity (*S*), we fit their marginal distributions with seven distributions shown in Table S2. The OR case (i.e., a bivariate drought event is identified with either a high severity or long duration) of the joint return period (JRP) under a Copula-based framework is used to quantify the occurrence of drought events (Yin et al., 2020). The joint distribution of drought duration and severity is constructed by using a Copula function, which is valuable for describing correlated hydrological variables (Li, 1999). Unlike univariate drought frequency analysis, the JRP within a bivariate framework can be represented by an isoline, which contains infinite combinations of values of these two multivariate arrays of variables. It is important for risk assessments to select a representative combination along the isoline. Previous studies have only selected joint design values according to the same frequency hypothesis that considering two correlated variables follow the same cumulative probability in their distributions, but this approach lacks a statistical basis and poorly describes the physical characteristics of droughts (Yin et al., 2018). In this paper, the joint probability density is used to optimize the most likely realization, which is mathematically expressed as follows:

$$\begin{cases} (d^*, s^*) = \arg\max f(d,s) = c[F_d, F_s] \bullet f_d \bullet f_s \\ C[F_d, F_s] = 1 - \mu / T_{or} \\ c[F_d, F_s] = \dfrac{dC(F_d, F_s)}{d(F_d)d(F_s)} \end{cases} \quad (14)$$

where $c[F_d, F_s]$ is the Copula probability density function; f_d and f_s are the fitted probability density functions of *D* and *S*, respectively; F_d and F_s are the marginal distribution of *D* and *S*, respectively; (d^*, s^*)

is the most likely realization under a given JRP T_{or} ; μ is the mean inter-arrival time between two consecutive droughts.

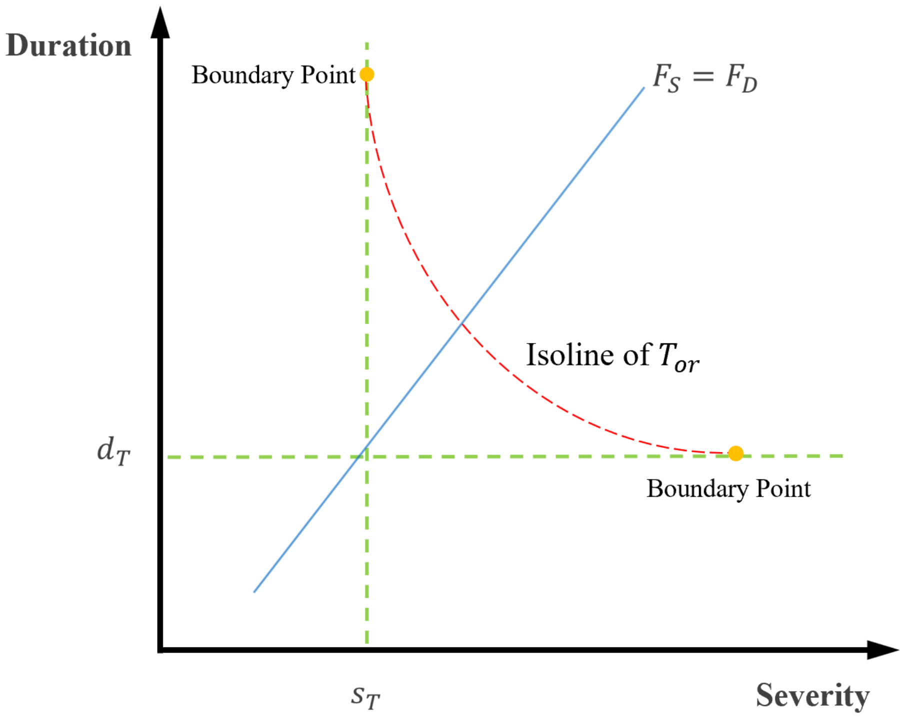

Figure 3. Joint distribution of drought duration and severity under a critical T_{or}. The green lines are two arbitrary values of duration and severity. The red line is the isoline line of two variables under a critical T_{or}, and the blue line denotes the traditional equal-frequency assumption. The d_T and s_T are marginal distribution quantiles for a given probability level T; F_S and F_D are cumulative probability density of severity and duration, respectively. T_{or} is a given probability level under the OR case.

The future socioeconomic exposure after 2020s has directly been defined as ranging from 0 to 100% (Gu et al., 2020a), but dynamically shifting climate risks cannot be represented under this definition, without considering fluctuation in the frequency of hazards. Here, the socioeconomic exposure is defined by considering the shift in JRP, and is expressed at the catchment scale as follows:

$$E_{POP} = \frac{T_h I(T_h - T_f)}{T_f A_d} \times POP \tag{15}$$

$$E_{GDP} = \frac{T_h I(T_h - T_f)}{T_f A_d} \times GDP \tag{16}$$

where E_{POP} and E_{GDP} denote the population and GDP exposure; T_h and T_f denote the historical and future JRP, respectively; $I(\cdot)$ denotes the controlling function, which is 1 when $T_h - T_f < 0$, or 0 when $T_h - T_f \geq 0$ is recorded; *POP* and *GDP* denote the population and the gross domestic product (in USD) of a given catchment in the future climate, respectively.

2.6 Quantifying the uncertainty contributed by different sources

Uncertainties in the future drought projections can arise from the SSPs, GCMs and HTMs. During both historical (1985-2014) and future periods (2071-2100), the combination of 3 SSPs, 5 GCMs and 10 HTMs through the impact modeling chain resulted in 150 hybrid combinations. The overall uncertainty is calculated from the variance of the future estimated JRP relative to the historical 50-year droughts. To partition the uncertainty from different sources of data and their interaction effects, the MANOVA is used and expressed as follows (Weinfurt, 1995):

$$\Delta y_{x,y,z} = M + S_x + G_y + H_z + I_{x,y,z} \tag{17}$$

where M denotes the mean change of all indicators in models; S_x, G_y and H_z denote the impact on indicators of the x^{th} SSP, y^{th} GCM and z^{th} HTM, respectively; $I_{i,j,k}$ is the overall impact arising from the interactions of different sources. The overall variance V is then expressed as follows:

$$V = VS + VG + VH + VI_{SG} + VI_{SH} + VI_{GH} + VI_{SGH} \tag{18}$$

where VS, VG, VH are the variance from the SSPs, GCMs and HTMs, respectively. VI_{SG}, VI_{SH}, VI_{GH} and VI_{SGH} denote the variance caused by the coupling between different sources of data. The contribution of each source to the overall uncertainty is quantified by the variance of each source to the total variance.

3. Data and materials

3.1 In situ observation dataset

We use a gridded meteorological dataset with 0.5° × 0.5° resolution, including daily temperature (maximum, minimum and average, °C) and daily precipitation (mm) from 1961 to 2018, provided by the National Meteorological Bureau of China. The dataset is regarded as the latest gridded meteorological dataset in China and has been applied to some studies (e.g., Wu et al., 2018; Yin et al., 2021a,b). Meanwhile, we gathered the daily streamflow of 463 in situ hydrological stations spanning different periods during 1961-2018. The hydrological stations are densely distributed in East China, while West China has a sparser distribution. Through rigorous data quality checks, 179 unnested basins with at least 20 years of data were selected, covering nine major watersheds in China. For more details on streamflow data processing and catchment screening, please refer to Yin et al. (2021b).

3.2 GRACE/GRACE-FO measurements

Temporal variations in the Earth's gravitational field observed by GRACE satellites have been used to retrieve TWS data (Tapley et al., 2004). Many international institutes have released the TWS mascon products at a monthly scale, including the JPL (Jet Propulsion Laboratory of the California Institute of Technology), the GSFC (Goddard Space Flight Center of NASA), and the CSR (Center for Space Research of the University of Texas). As these three mason solutions are produced at different spatial resolutions, we generated blended TWS data based on the average of JPL, GSFC and CSR with 0.5°×0.5° resolution from 2002 to 2022, and fill the missing data using a linear interpolation approach (Yin et al., 2022).

3.3 ERA5-Land dataset

ERA5-Land is a dataset that consists of a large volume of meteorological variables, including precipitation, temperature, air pressure etc. The spatial resolution of the dataset is 9 km and the temporal resolution is one hour (Yilmaz, 2023). Under the latest global reanalysis and the lapse rate correction, the ERA5-Land reanalysis dataset provides a substitute for unavailable observed weather data, by taking the effect of altitude on the spatial scheme of climate variables into consideration (Pelosi et al., 2020). Six variables are used in the study (i.e., *pr*, *ps*, T_{2m}, T_d, *srlds*, *srsds*) and aggregated to a daily scale from the hourly scale before conducting data analysis.

3.4 Bias-corrected GCM outputs and socioeconomic scenarios

The climate outputs of five GCMs of the historical scenario and three SSPs (i.e., SSP1-26, SSP3-70, SSP5-85) under CMIP6 are used to represent different climate scenarios. Generally, the SSP5-85 configured the highest carbon emission and human interference with the natural environment. The SSP3-70 and the SSP1-26 have progressively conservative changes to represent climate change resulting from different levels of human activity. The series of bias-corrected variables have been downscaled to 0.5° × 0.5°resolution from 1850 to 2100 under the Intersectoral Impact Model Intercomparison Project 3b (ISIMIP3b) (Lange, 2019). To reduce the systematical biases of CMIP6 raw outputs, seven variables from the bias-corrected ISMIP3b dataset have been used, namely temperature (daily average, maximum and minimum), *pr*, *ps*, *srsds*, *srlds*, *RH* and *SH*.

Population and GDP data under three SSPs are employed to evaluate the potential socioeconomic risks of drought in a warming world. An open-access population dataset is adopted which takes into consideration the universal two-child policy, the census results and the statistical annual report (Jiang et al., 2017). The economic index from 2010 to 2100 is estimated based on the Cobb-Douglas and Population-Environment-Development model (Jiang et al., 2018). All of the data have been previously used to assess the socio-economic impact of extreme hydrologic hazards (Yin et al., 2022; Yin et al., 2023).

4. Results

4.1 Observed changes in SRI and TWS-DSI based drought

As there are insufficient streamflow observations to compute the SRI in northwest China, we also employed the TWS-DSI as a supplement. This approach enriches the variety of water storage or flux being evaluated. Based on linear regression and least square method, trends in drought characteristics (i.e., frequency, duration and severity) are estimated by using the GRACE/GRACE-FO dataset and observed runoff across China. Figure 4 and Figure 5 show the drought trends based on the TWS-DSI and SRI, respectively. Overall, the two indexes show similar trends in most catchments, suggesting that drought hazards have increased during 2002-2022. TWS-DSI droughts have increased in 54% of areas, which are mainly located in the Qinghai-Tibet Plateau, the North China Plain and the northwestern Xinjiang Province. Likewise, SRI droughts have increased over 51% of studied catchments, which mainly dominate northeastern and southeastern China. The severity of droughts measured by the TWS-DSI index is twice of the hydrological drought, primarily because the TWS-DSI metric incorporates all vertical water fluxes, offering a comprehensive view of shifts in water scarcity. On the other hand, TWS-DSI can difficultly represent the aquifer recharge processes, which are fundamental physical process of baseflow and the hydrological drought in its entire extension. Therefore, catchments with aquifer recharge and storage capacity will exceed several times the time step of the analysis, enlarging the severity of droughts. Some locations exhibit discrepancies depending on the index considered. For instance, droughts in the Qinghai-Tibet Plateau and Northeast China show opposite trends. Anomalies in the Qinghai-Tibetan plateau may be explained by the transformation of snowpack melt into surface runoff under the influence of climate change, which helps compensate for the lack of surface water in the area (Stewart, 2009). The discrepancy observed in Northeastern China could potentially be linked to the rise in soil moisture from increased infiltration, which causes a higher proportion of water to be stored within the soil than at the surface, interfering with the quantification of hydrological drought (Wang et al., 2017). Finally, both indicators show a consistent positive drought trend in most areas of China and particularly the North China Plain and Pearl River Basin.

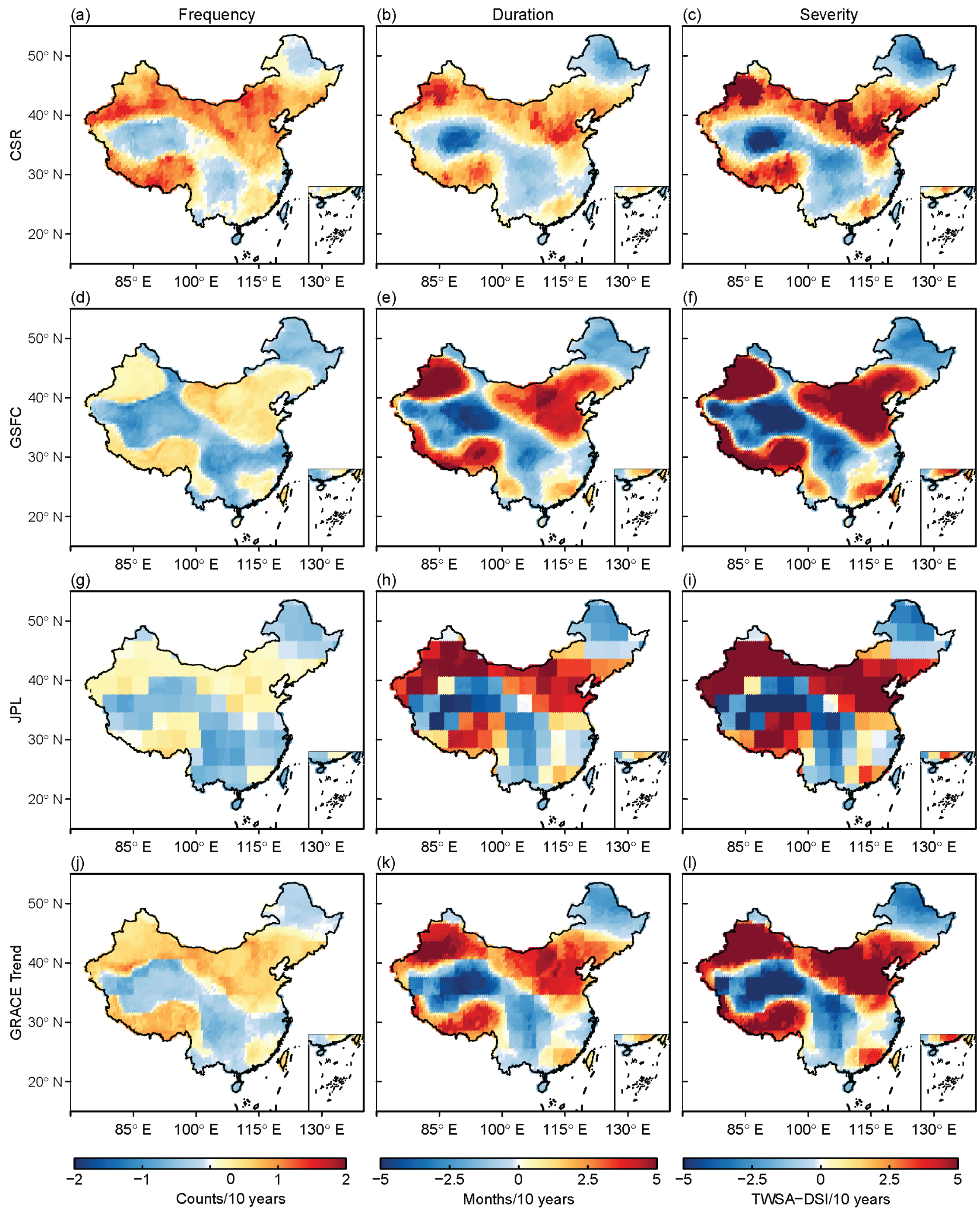

Figure 4. Trends in drought frequency, duration and severity based on the TWS-DSI from 2002 to 2022 using three GRACE/GRACE-FO products (a-i) and the blended data (j-l).

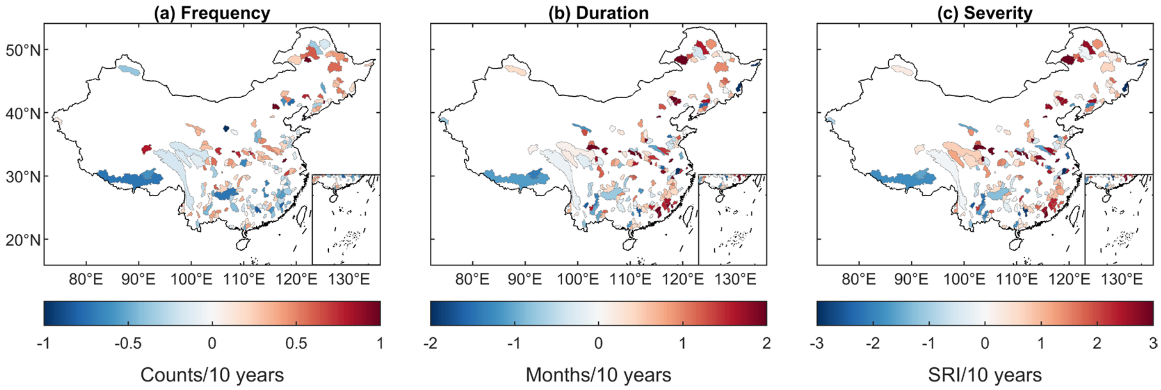

Figure 5. Trends in drought frequency, duration and severity from 2002 to 2022 over China. (c), the index of severity is based on the SRI statistic (Eq. 13).

4.2 Machine Learning-constrained streamflow simulation and model evaluation

The RF model was used to quantify the sensitivity of streamflow to different meteorological variables (Figure 6). Since a station can be attributed to catchments of different sizes, we only considered the largest catchment scales in analysis.We quantified the sensitivity of seven historical mean meteorological variables (i.e., *pr*, *ps*, *SH*, *RH*, *srlds*, *srsds*, temperature) to monthly streamflow in each grid. Due to the sparse number of observation stations in Northwestern China, the reliability of the sensitivity analysis for these regions is lower than that of the dense observed areas. Precipitation typically plays a major role in generating runoff in Southeast China, although *SH* plays the most important role in some regions such as Central, Southwest and Northeast China. Over 30% and 38% of stations show the *SH* sensitivity rate of >10% in Western and Northeastern China respectively, indicating the dominance of *SH* in these areas. In contrast, *RH* and shortwave radiation have a negative contribution to streamflow; especially shortwave radiation, which has a pronounced negative sensitivity in 394 stations probably due to enhanced evapotranspiration (Ma et al., 2019). These negative contributions mean enhancement of these two variables will inhibit the generation of streamflow, showing the potential adverse effects of climate change on streamflow generation. In general, *RH* contributes to increasing streamflow over most regions of China, but the opposite effect is observed in 179 stations mainly located in Southwestern China, Yellow River and Huaihe River basins. This is the result of the mutual feedback of water and heat dynamics (i.e., saturated vapor pressure increases with warming and intensifies evaporation, leading to a decrease in surface water), which was also found by Liu et al. (2017). The temperature has a positive contribution to streamflow generation in Northeast China, suggesting a potential mitigation for the deficiency of surface flow. However, there is interactive feedback between hydrological and thermal factors that result in an inability to directly assess the impact of temperature on hydrologic droughts (Fig. 6i and 6f).

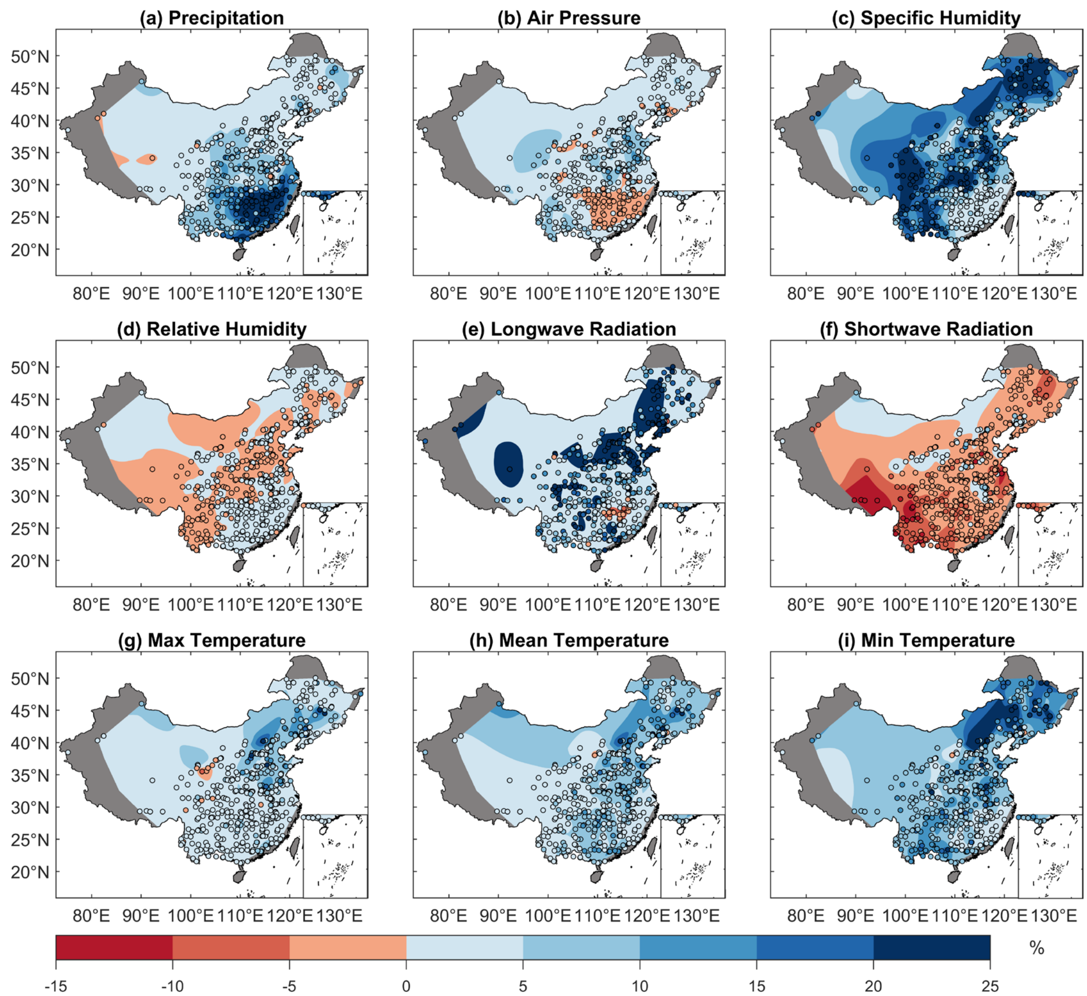

Figure 6. Sensitivity of meteorological variables to daily streamflow. The figure uses a thin plate smoothing spline method to interpolate the point-based station data (circles). Gray areas indicate missing data.

The performances of simulated streamflow by different HTMs are shown in Figure 7. The model that has the largest Kling-Gupta efficiency (KGE) is considered to be the best-performing in each catchment. In Fig 7. (a) and (b), the GR4J and GR4J-LSTM performed best in 77 out of 179 studied catchments. The median KGE value of GR4J is higher than 0.83, revealing a superior performance than the other hydrological models. Subsequently, the XAJ and XAJ-LSTM are the best models in 57 catchments, mainly located in the southern Yangtze River. Last, the HBV and HBV-LSTM performed best in only 10 catchments, where the streamflow are impacted by snowfall in plateaus and northern frozen areas. All catchments exhibit KGE values greater than 0.9 during the calibration period in Figure 7c, showing good performance in simulation. During the validation period, only 18 catchments have KGE values below 0.6, and most of the catchments have KGE values greater than 0.8 in Figure 7d. In summary, the trained models simulate streamflow well in all the studied catchments. Additionally, the KGE values in the southern region are generally higher than those in the northern region during the validation period, which is consistent with previous hydrological simulation works (Gu et al., 2020b, 2021). This phenomenon may be attributed to the higher dependence of streamflow on rainfall in South China, which is governed by a humid climate pattern (Zheng et al., 2022).

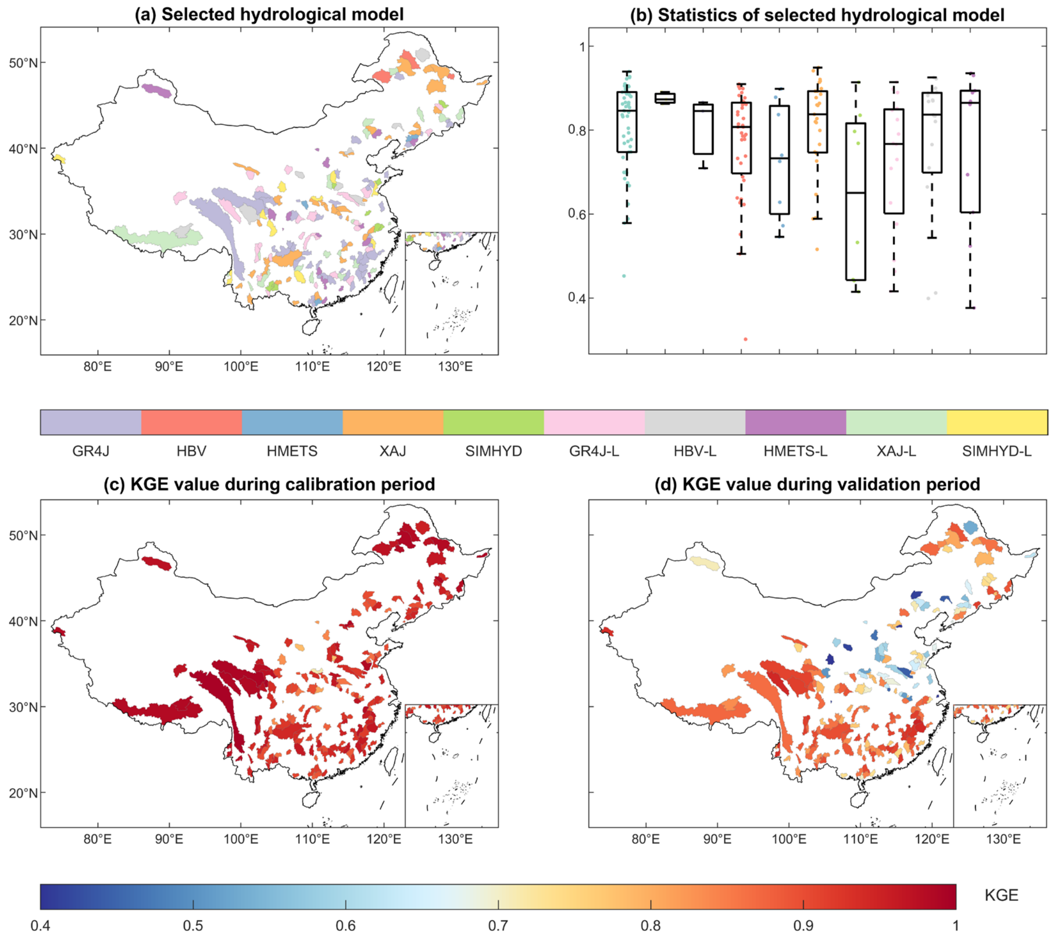

Figure 7. Hydrological simulation performances of all candidate models. (a), The best-performing model with the highest KGE value. The catchments are colored according to the best performing models. (b), Boxplots of all catchments for ten HTMs indicated by KGE values. (c)-(d), The highest KGE values during the calibration (c) and validation (d) period, respectively.

4.3 Projected changes in univariate drought characteristics

We projected the future daily runoff series by driving the HTMs with the bias-corrected CMIP6 variables, and then we estimated the monthly SRI to identify drought duration and severity. Based on the maximum Bayesian Information Criterion (BIC), we selected the best-performing marginal distributions for duration and severity from seven candidate distributions shown in Table S2, based on historical data for each catchment. Figure 8 and Figure 9 show the multi-model ensemble average severity and duration for the 50-year historical return period (RP).

In western China, we projected a significantly increasing drought trend under the three SSPs, which indicates potential for increased water scarcity and more frequent extreme drought events. In Southeast China, we projected that drought events are likely to intensify under SSP3-70 but not under SSP5-85. It is generally considered that SSP5-85 is accompanied by higher carbon emissions than that of SSP3-70 (O'Neill et al., 2016). However, future works also take significant action to control the extent of climate change combined with strong climate policies under SSP5-85 (Fujimori et al., 2017). As a result, there is no deterioration of drought severity with policy interventions, which emphasizes the significance of ensuring the implementation of climate strategies. In northern China, in contrast, we found that future drought risks are projected to decrease under the three scenarios, which is possibly related to more moisture convergence from the East Asian monsoon circulation as the warming climate (Chowdary et al., 2019).

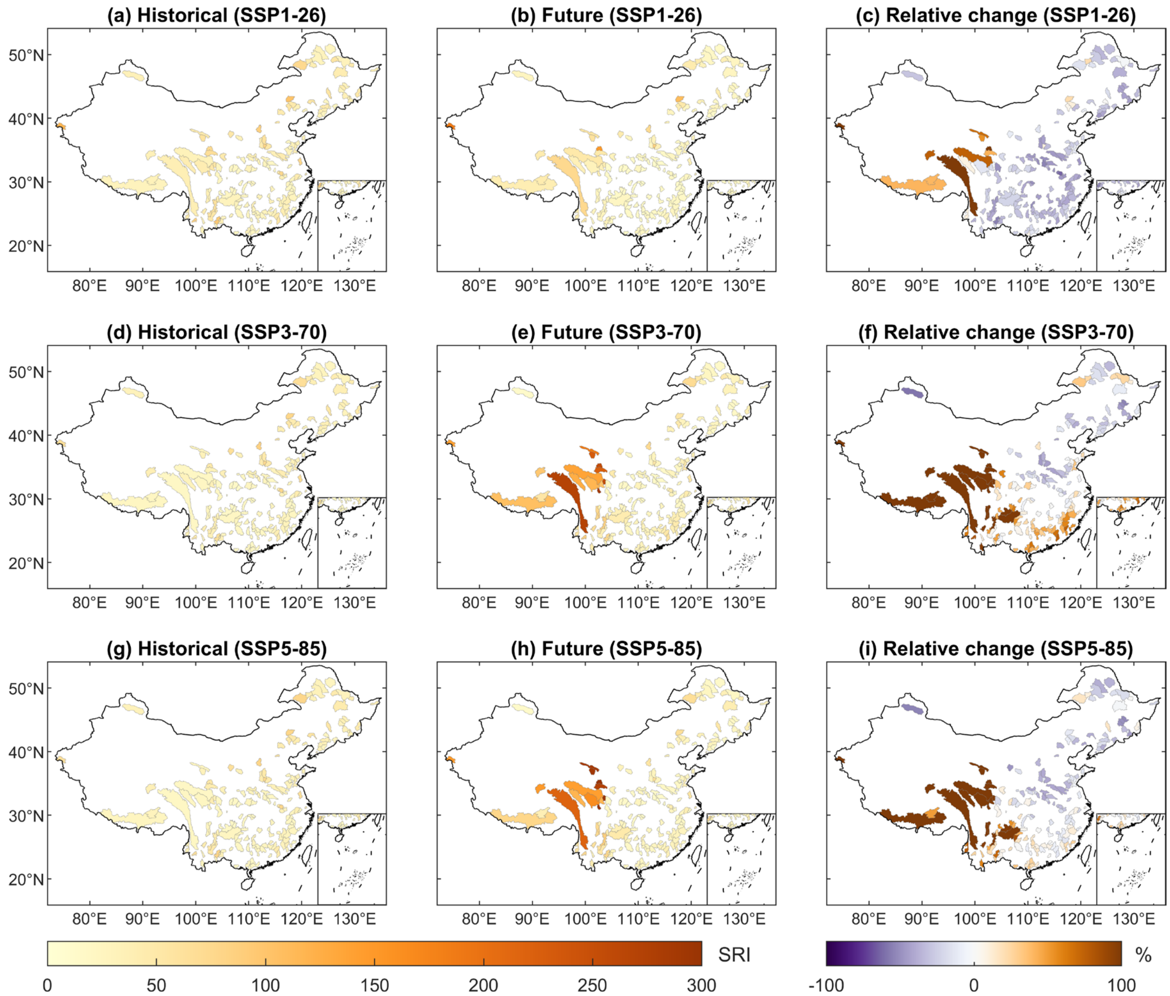

Figure 8. Multi-model ensemble average design severity (dimensionless) under a 50-year RP for three SSPs, and relative changes (%) in 2071-2100 compared to 1985-2014.

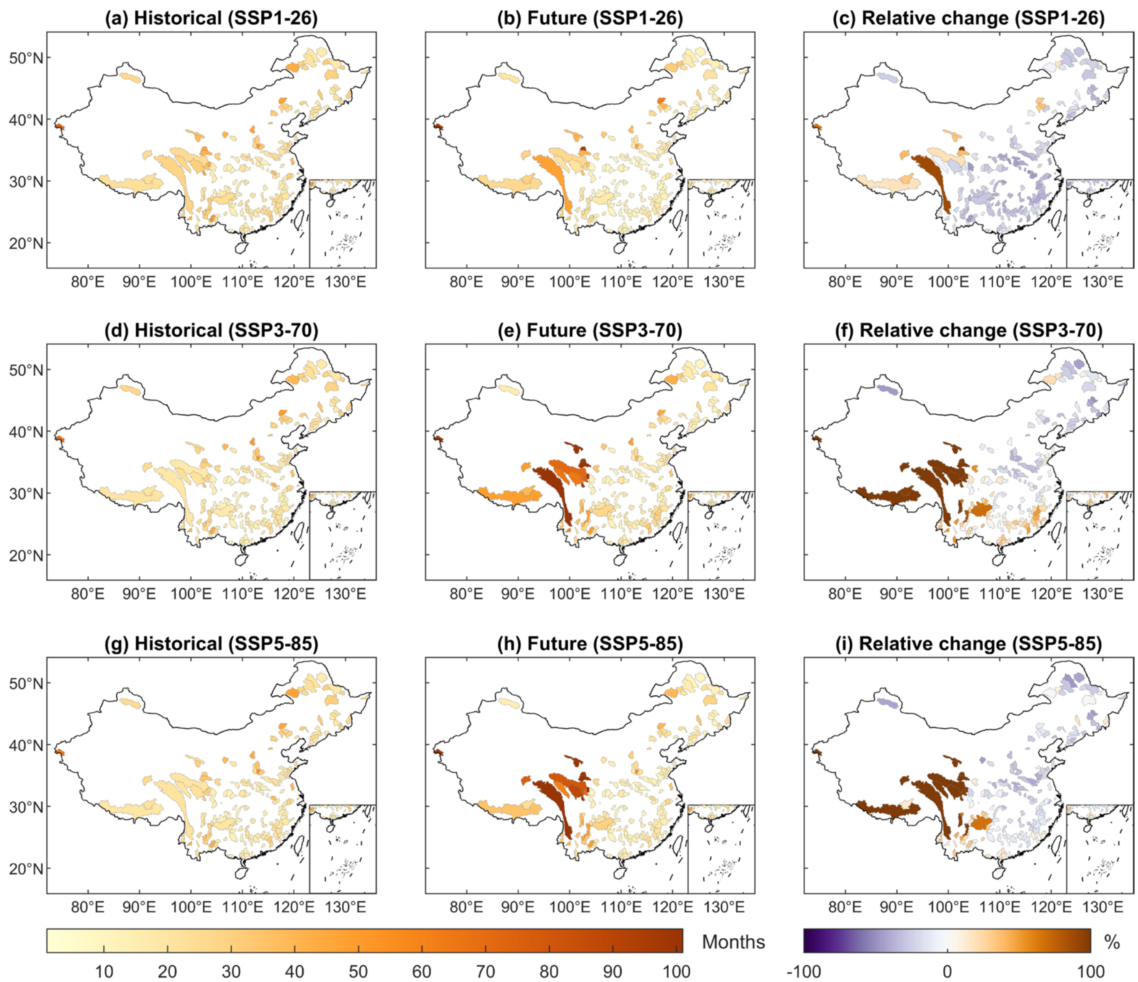

Figure 9. Multi-model ensemble average design duration (months) of the multi-model for a 50-year RP for three SSPs, and relative changes (%) in 2071-2100 compared to 1985-2014.

We display the relative change of drought characteristics under 50-year RP for all catchments for five GCMs under the three SSPs using violin plots (Figure 10). For most catchments, the relative change of drought duration and severity is negative. However, the relative change under some scenarios reached a maximum of 400%, highlighting the extreme change of drought. The median relative change of severity based on the IPSL-CM6A-LR under SSP3-70 are 30%, and 22% of catchments have a relative change over 200%, representing the most severe case of drought evolution. Furthermore, the distributions of the projections based on the MPI-ESM1-2-HR, MRI-ESM2-0 and UKESM1-0-LL models are highly skewed and bimodal under SSP3-70 and SSP5-85, revealing substantial spatial heterogeneity across China. Overall, the severity and duration of droughts slightly increase in some catchments and have the risk of extreme intensification as a result of global warming.

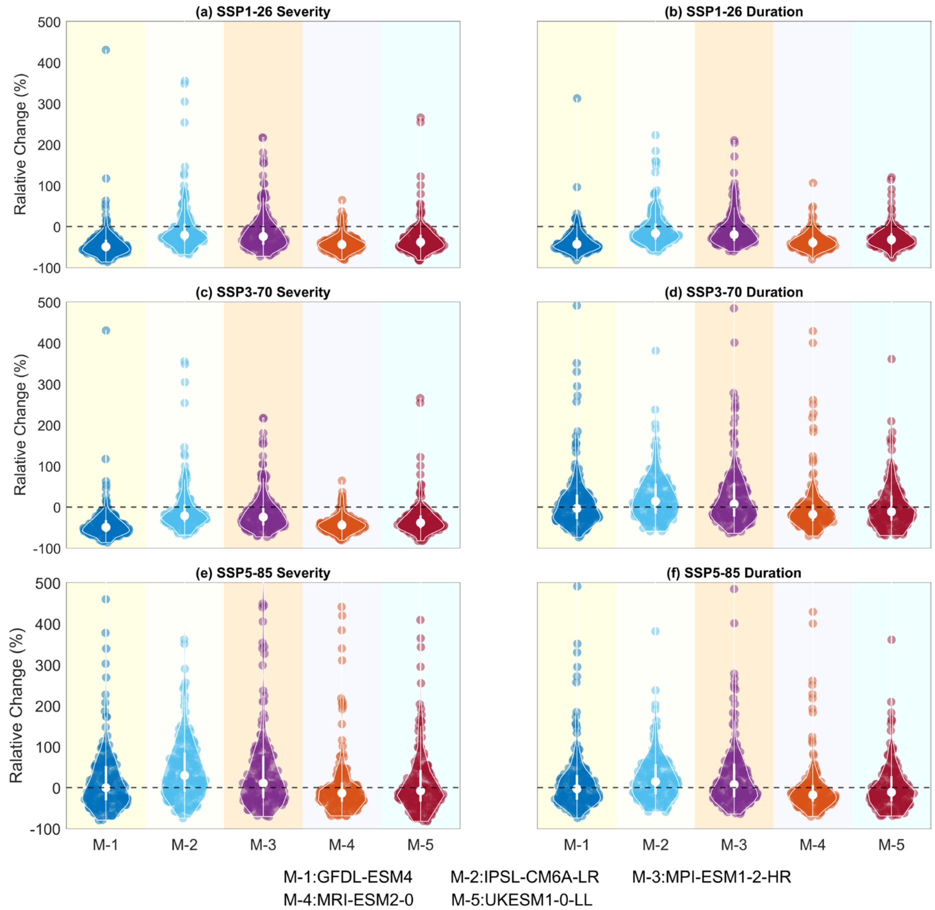

Figure 10. Violin plots of relative changes (%) in severity and duration to the historical drought event with 50-year RP under three SSPs. The white circles are the median values of relative changes.

4.4 Bivariate drought changes and corresponding socioeconomic risks

To capture the complex dependence structure between drought severity and duration, we used a Copula function to quantify the bivariate risk of hydrological droughts under climate change. Changes in the JRP of the historical (1985-2014) drought event with 50-year JRP in the future (2071-2100) period are shown in Figure 11. The medians of the projected future JRP are 38.78 years, 14.52 years and 19.24 years under SSP1-26, SSP3-70 and SSP5-85, respectively. For 69% and 60% catchments under SSP3-70 and SSP5-85, we find the JRP of the 50-year drought is reduced to less than 25 years in the future period, suggesting that the risk of drought increases over 2 times in these catchments. Besides, we find a marked increase in the number of catchments with increased drought risk compared to the univariate drought assessments. The JRP of catchments in Northeastern and Central China tends to decrease, suggesting higher changes in risks than univariate assessments. This result is consistent with previous studies (He et al., 2011; Xu et al., 2015), which indicates that the use of bivariate drought analysis can amplify the individual effects of two drought characteristics.

Future GDP and population exposed to increasing bivariate drought risk under three scenarios are shown in Figure 12. The eastern coastal regions have a higher significant economic exposure such as the Huaihe

River Basin, the Yangtze River Basin and the Pearl River Basin, which is consistent with the distribution of economically developed regions in China. The medians of GDP exposure are 5.5, 9.8 and 14.3 million dollars/km^2 under three SSPs respectively, which indicates the vulnerability of economic losses to drought disasters under global warming. The population affected by drought is mainly located in the southern Yangtze River Basin and the Huaihe River Basin under SSP3-70, as the median exposure is 525 and 205 people/km^2 under SSP3-70 and SSP5-85, respectively. This is because the increase in population is higher in the Sichuan, Guangdong and Zhejiang provinces than in other Chinese provinces under SSP3-70 (Chen et al., 2020). Overall, the exposure of GDP and population shows large heterogeneity in their sensitivity to different scenarios, and the distribution of the affected catchments is consistent with economic and social development.

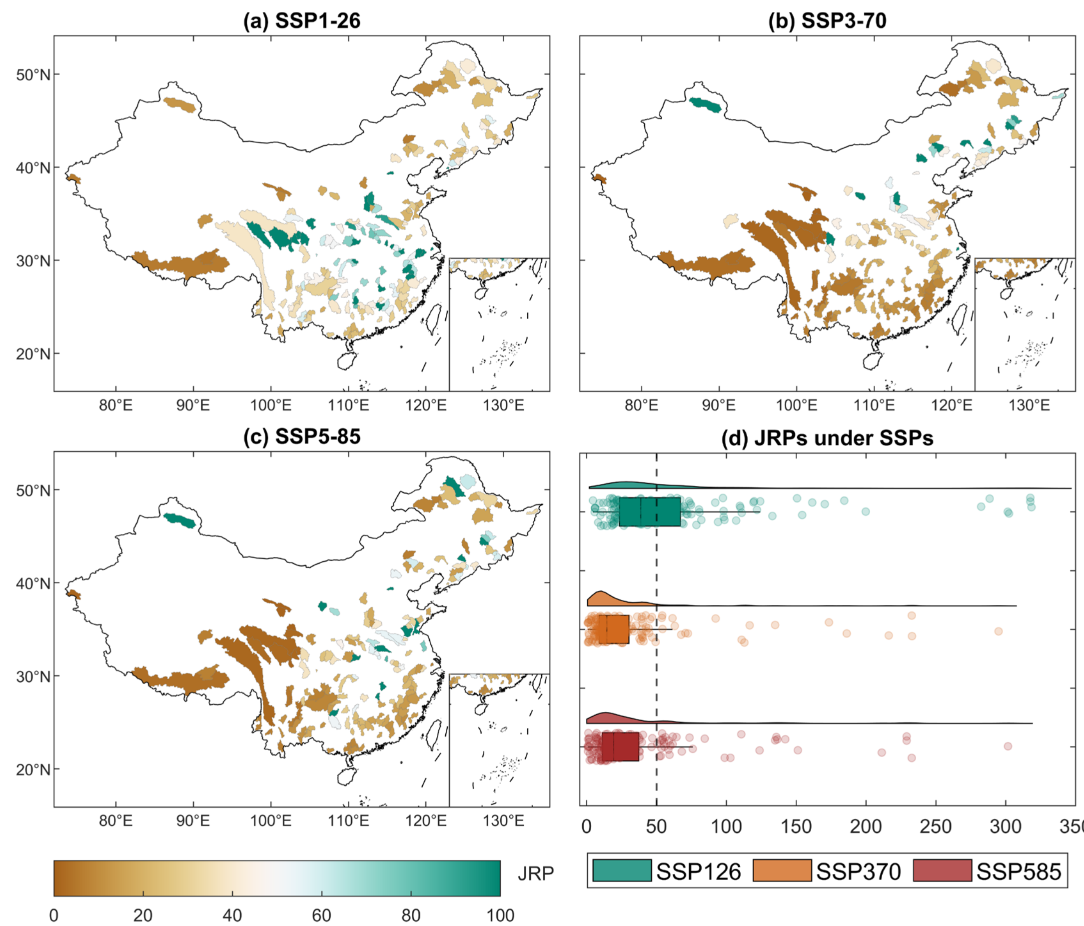

Figure 11. The future multi-model ensemble means JRP of the historical drought with a 50-year T_{or} based on the bivariate approach. The future JRPs of 179 catchments under three SSPs are presented in (a)-(c), while (d) displays raincloud plots of the projected JRP under each SSP.

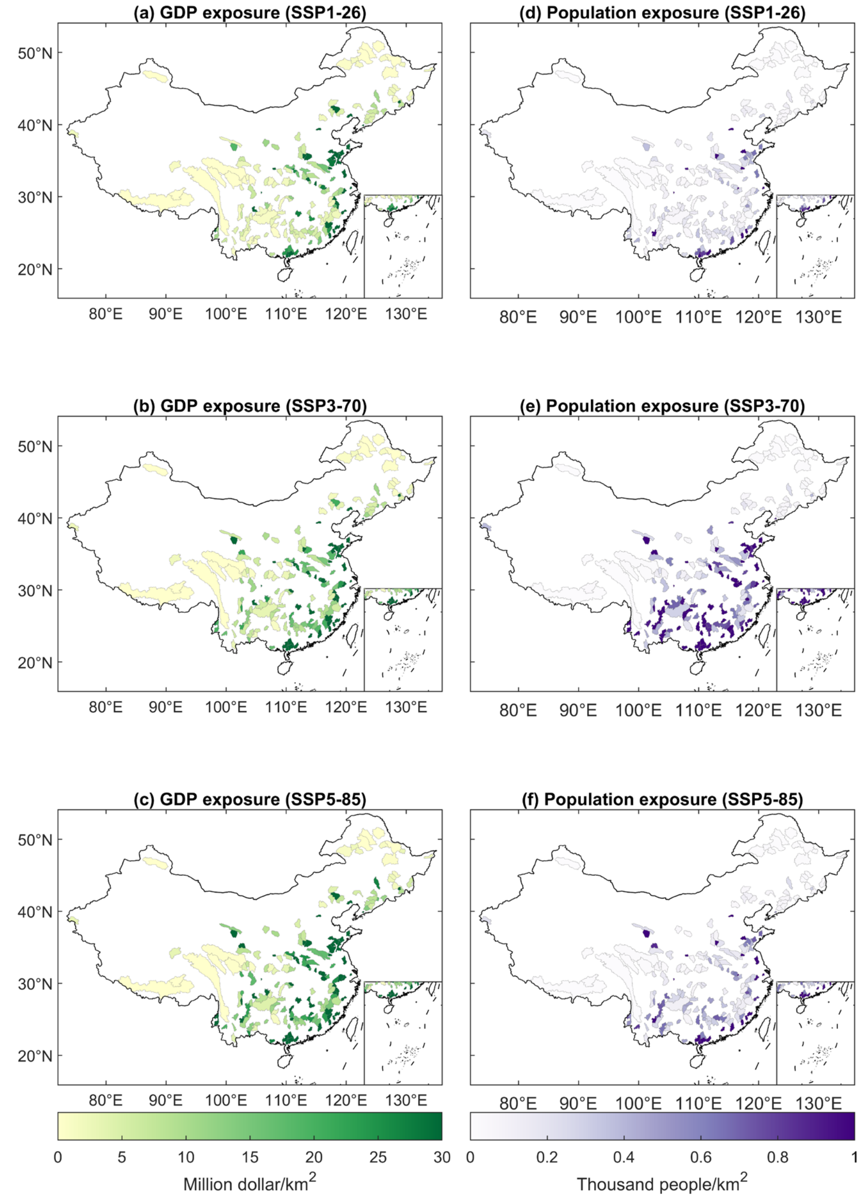

Figure 12. The multi-model ensemble means exposure of GDP (a-c) and population (d-f) to bivariate drought characteristics under different SSPs in the future period.

5. Discussion

5.1 Uncertainty decomposition

The overall uncertainty in our projections arises from the different SSPs, GCMs and HTMs as well as their interactions. We assemble these seven sources using MANOVA (Figure 13). For GDP and POP exposure, we find HTM is the main source of uncertainty, and contributes 27.55% and 26.14% uncertainty, respectively. This indicates that the quality of the HTM is important for the accuracy of socioeconomic predictions. Likewise, the GCM and GCM-HTM provide over 30% of the uncertainty in GDP and population exposures, which indicates the critical importance of bias-corrected GCM outputs for accurate projections. Further, the contributions of the SSPs to population exposure is 1.5 times than that of GDP exposure, which shows that the effect of climate change is greater for POP exposure than GDP exposure. In particular, the independent factors (i.e., SSP, GCM, HTM) contribute over 50% to the uncertainty of GDP and population exposures, suggesting that GDP and population exposures are less responsive to complex coupling. In contrast, the coupled factors (i.e., the combination of SSP, GCM or HTM) mainly contribute to the uncertainty of the JRP, accounting for 82.63% of the overall uncertainty, especially the SSM-GCM-HTM, which accounts for 36.97% of uncertainty. Finally, the relatively low contribution of the choice of SSP, SSP-GCM and SSP-HTM to JRP uncertainty indicates that the future risk projection uncertainty is relatively stable in future risk projections

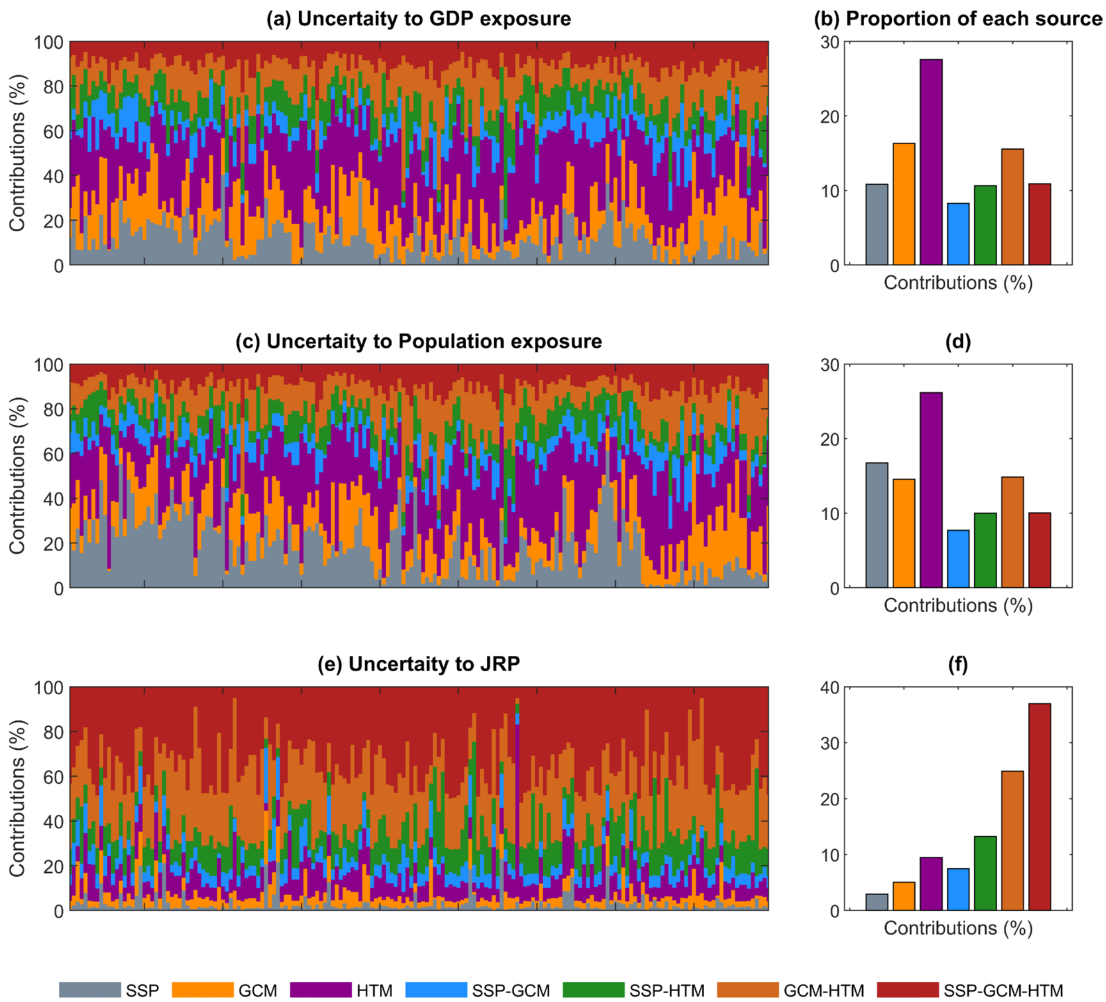

Figure 13. The fractional uncertainty contributions of all sources to the GDP exposure, population exposure, and JRP estimate for all 179 catchments (a, c, e) and the average fractional contribution of each source (b, d, f).

5.2 Limitations and future work

The uncertainty caused by the underlying surface situation and the coupling relationships behind interrelated variables remains unexplained in this study. Therefore, revealing interactions among multisource data is important to understand how the drivers affect the water cycle under climate change. Here, only five

GCM outputs and one in situ observation dataset were used to drive our HTM models. The sparse dataset may undermine the robustness of the approach. Providing a larger number of GCMs and observational data to assemble a more sophisticated model might be an effective approach to improve accuracy and reliability. Although the catchments gathered in this study cover nine major watersheds in China, there is still a requirement for streamflow data with a more uniform spatial density. Considering geospatial sampling techniques, a homogeneous density of catchments is significant to reveal the spatial distribution of drought. On the other hand, due to the heterogeneity of different climatic regions in China, we would like to expand hydrological models (e.g., the weather research and forecasting model hydrological modeling system, soil and water assessment tool or the hydrological modules of land surface process models) to reduce uncertainty in future research. Finally, the GDP and population projections cannot well reflect future economic development and population migration, especially the governmental intervention in immigration and economic policies. It is better to consider the dynamic impact of human management on socioeconomic development, which is essential for the construction of a more reliable projection framework.

5.3 Suggestions for drought mitigation in China

In order to curb global warming and mitigate the threats of climate change, the Chinese government is striving to reach its carbon peak before 2030, achieve carbon neutrality before 2060, and bolster efforts in disaster reduction (Kundzewicz et al., 2019; Liu et al., 2022b). China has nonetheless experienced several extreme drought events during the past 5 years, threatening the population’s health and economic development (Ding and Gao, 2020; Liu et al., 2022a; Mallapaty, 2022). The Intergovernmental Panel on Climate Change (IPCC) has emphasized that projections of future climate trends can equip policymakers with the scientific insight needed to navigate the challenges of climate change (Pörtner et al., 2022). The results of this study aim to alert policymakers to drought risk in Southwestern China which was just hit by severe drought events and expected to significantly intensify with climate change. We strongly highlight the importance of strictly implementing carbon emission reduction initiatives and developing prevention programs to limit potential drought losses. Preserving local ecological balance and employing rational use of water resources could be the key to mitigating potential losses from extreme droughts (Chang et al., 2019; Sohn et al., 2016). Although China has constructed hydraulic structures with a total water storage capacity of over 7,064 billion m3, current irrigation facilities need to expand to mitigate the challenge of drought under climate change (Cai et al., 2015; Xiao-jun et al., 2012). In addition, it is also beneficial for policymakers that establish a drought information system to get a comprehensive collection of drought impacts from all potential sectors, which can link the government and research organizations (Wilhite et al., 2007).

The Intergovernmental Panel on Climate Change (IPCC) has emphasized that projections of future climate trends can equip policymakers with the scientific insight needed to navigate the challenges of climate change (Pörtner et al., 2022). The results of this study aim to alert policymakers to drought risk in Southwestern China, which is expected to intensify with climate change. Preserving local ecological balance and employing rational use of water resources could be the key in mitigating potential losses from extreme droughts (Chang et al., 2019; Sohn et al., 2016). Finally, this work highlights the importance of strictly implementing carbon emission reduction initiatives and developing prevention programs to limit potential drought losses.

6. Conclusions

In this study, the hybrid LSTM-constrained hydrological models show high efficiency in studied catchments over China, demonstrating that machine learning can effectively constrain the hydrological simulation. Projected changes in 50-year bivariate drought characteristics, expressed as a JRP, indicate that the risk of hydrological drought is likely to more than double in over 60% of catchments by the end of the 21^{st} century under SSP5-85. The spatial distribution of change reveals that the catchments with severely increased drought risk are mainly located in southwestern China. Notably, the exposure of GDP and population varies greatly across different SSPs. The median GDP exposure under SSP5-85 is 1.5 times that of SSP3-70, but the median population exposure is just 40% that of SSP3-70. The higher population exposure under SSP3-70 can be attributed to rapid population growth. Finally, we find the interaction between multiple sources of data explains more than 80% of the uncertainty in future changes in JRPs, showing the importance of considering the relationships between model components. Our findings demonstrate that China will face higher drought risks in a warmer future, emphasizing the urgency of implementing strategies to reduce carbon emissions. Our study is insufficient in the revelation of drought hazard drivers and needs to expand datasets and hydrological models to promote the reliability of simulation in future studies. We would also like to take governmental interference of economic and demographic policies into consideration.

Data availability

The gridded meteorological dataset for China can be obtained from http://www.cma.gov.cn. The ISIMIP3b data can be downloaded from https://data.isimip.org. The ERA5-Land data can be downloaded from https://www.ecmwf.int/en/era5-land. Streamflow simulations used in this study are available at https://osf.io/fvyse/.

Acknowledgments

J.Y. acknowledges support from the National Natural Science Foundation of China (Grant NOs. 52361145864; 52261145744). L.S. is supported by UKRI (MR/V022008/1). J.G. is supported by the National Natural Science Foundation of China (NO. 52179018). This work is also supported by the Undergraduate Training Programs for Innovation and Entrepreneurship of Wuhan University. The numerical calculations in this paper have been performed on the supercomputing system in the Supercomputing Center of Wuhan University.

Competing interests

At least one of the (co-)authors is a member of the editorial board of Hydrology and Earth System Sciences.

References

Allan, R. P., Barlow, M., Byrne, M. P., Cherchi, A., Douville, H., Fowler, H. J., Gan, T. Y., Pendergrass, A. G., Rosenfeld, D., Swann, A. L. S., Wilcox, L. J., and Zolina, O.: Advances in understanding large-scale responses of the water cycle to climate change, Annals of the New York Academy of Sciences, 1472, 49–75, https://doi.org/10.1111/nyas.14337, 2020.

Antoniadis, A., Lambert-Lacroix, S., and Poggi, J.-M.: Random forests for global sensitivity analysis: A selective review, Reliability Engineering & System Safety, 206, 107312, 2021.

Arsenault, R., Essou, G. R., and Brissette, F. P.: Improving hydrological model simulations with combined multi-input and multimodel averaging frameworks, Journal of Hydrologic Engineering, 22, 04016066, 2017.

Ashrafi, S. M., Gholami, H., and Najafi, M. R.: Uncertainties in runoff projection and hydrological drought assessment over Gharesu basin under CMIP5 RCP scenarios, Journal of Water and Climate Change, 11, 145–163, 2020.

Ayantobo, O. O., Li, Y., Song, S., and Yao, N.: Spatial comparability of drought characteristics and related return periods in mainland China over 1961–2013, Journal of Hydrology, 550, 549–567, 2017.

Barker, L. J., Hannaford, J., Chiverton, A., and Svensson, C.: From meteorological to hydrological drought using standardised indicators, Hydrology and Earth System Sciences, 20, 2483–2505, 2016.

Bergström, S.: The HBV model, Computer models of watershed hydrology, 443–476, 1995.

BERGSTRÖM, S. and FORSMAN, A.: DEVELOPMENT OF A CONCEPTUAL DETERMINISTIC RAINFALL-RUNOFF MODEL, Hydrology Research, 4, 147–170, 1973.

Berne, A., Delrieu, G., Creutin, J.-D., and Obled, C.: Temporal and spatial resolution of rainfall measurements required for urban hydrology, Journal of Hydrology, 299, 166–179, 2004.

Byakatonda, J., Parida, B. P., Moalafhi, D. B., and Kenabatho, P. K.: Analysis of long term drought severity characteristics and trends across semiarid Botswana using two drought indices, Atmospheric research, 213, 492–508, 2018.

Cai, X., Zeng, R., Kang, W. H., Song, J., and Valocchi, A. J.: Strategic Planning for Drought Mitigation under Climate Change, Journal of Water Resources Planning and Management, 141, 04015004, https://doi.org/10.1061/(ASCE)WR.1943-5452.0000510, 2015.

Castle, S. L., Thomas, B. F., Reager, J. T., Rodell, M., Swenson, S. C., and Famiglietti, J. S.: Groundwater depletion during drought threatens future water security of the Colorado River Basin, Geophysical research letters, 41, 5904–5911, 2014.

Catani, F., Lagomarsino, D., Segoni, S., and Tofani, V.: Landslide susceptibility estimation by random forests technique: sensitivity and scaling issues, Natural Hazards and Earth System Sciences, 13, 2815–2831, https://doi.org/10.5194/nhess-13-2815-2013, 2013.

Chang, J., Guo, A., Wang, Y., Ha, Y., Zhang, R., Xue, L., and Tu, Z.: Reservoir operations to mitigate drought effects with a hedging policy triggered by the drought prevention limiting water level, Water Resources Research, 55, 904–922, 2019.

Chen, H. and Sun, J.: Increased population exposure to extreme droughts in China due to 0.5 °C of additional warming, Environ. Res. Lett., 14, 064011, https://doi.org/10.1088/1748-9326/ab072e, 2019.

Chen, J., Li, C., Brissette, F. P., Chen, H., Wang, M., and Essou, G. R.: Impacts of correcting the inter-variable correlation of climate model outputs on hydrological modeling, Journal of hydrology, 560, 326–341, 2018.

Chen, Y., Guo, F., Wang, J., Cai, W., Wang, C., and Wang, K.: Provincial and gridded population projection for China under shared socioeconomic pathways from 2010 to 2100, Scientific Data, 7, 83, https://doi.org/10.1038/s41597-020-0421-y, 2020.

Chen, Z. and Yang, G.: Analysis of drought hazards in North China: distribution and interpretation, Nat Hazards, 65, 279–294, https://doi.org/10.1007/s11069-012-0358-3, 2013.

Chiew, F. H. S., Peel, M. C., and Western, A. W.: Application and testing of the simple rainfall-runoff model SIMHYD., Mathematical models of small watershed hydrology and applications, 335–367, 2002.

Cho, K., Van Merriënboer, B., Gulcehre, C., Bahdanau, D., Bougares, F., Schwenk, H., and Bengio, Y.: Learning phrase representations using RNN encoder-decoder for statistical machine translation, arXiv preprint arXiv:1406.1078, 2014.

Chowdary, J. S., Hu, K., Srinivas, G., Kosaka, Y., Wang, L., and Rao, K. K.: The Eurasian jet streams as conduits for East Asian monsoon variability, Current Climate Change Reports, 5, 233–244, 2019.

Dai, A., Zhao, T., and Chen, J.: Climate Change and Drought: a Precipitation and Evaporation Perspective, Curr Clim Change Rep, 4, 301–312, https://doi.org/10.1007/s40641-018-0101-6, 2018.

Dikici, M.: Drought analysis with different indices for the Asi Basin (Turkey), Sci Rep, 10, 20739, https://doi.org/10.1038/s41598-020-77827-z, 2020.

Dikshit, A., Pradhan, B., and Huete, A.: An improved SPEI drought forecasting approach using the long short-term memory neural network, Journal of environmental management, 283, 111979, 2021a.

Dikshit, A., Pradhan, B., and Alamri, A. M.: Long lead time drought forecasting using lagged climate variables and a stacked long short-term memory model, Science of The Total Environment, 755, 142638, 2021b.

Ding, T. and Gao, H.: The record-breaking extreme drought in Yunnan Province, Southwest China during spring-early summer of 2019 and possible causes, Journal of Meteorological Research, 34, 997–1012, 2020.

Dixit, S., Atla, B. M., and Jayakumar, K. V.: Evolution and drought hazard mapping of future meteorological and hydrological droughts using CMIP6 model, Stochastic Environmental Research and Risk Assessment, 36, 3857–3874, 2022.

Donat, M. G., Lowry, A. L., Alexander, L. V., O'Gorman, P. A., and Maher, N.: More extreme precipitation in the world's dry and wet regions, Nature Climate Change, 6, 508–513, 2016.

Duan, Q., Sorooshian, S., and Gupta, V.: Effective and efficient global optimization for conceptual rainfall-runoff models, , 28, 1015–1031, 1992.

Fujimori, S., Hasegawa, T., Masui, T., Takahashi, K., Herran, D. S., Dai, H., Hijioka, Y., and Kainuma, M.: SSP3: AIM implementation of shared socioeconomic pathways, Global Environmental Change, 42, 268–283, 2017.

Ganguli, P. and Merz, B.: Trends in compound flooding in northwestern Europe during 1901–2014, Geophysical Research Letters, 46, 10810–10820, 2019.

Gers, F. A., Schmidhuber, J., and Cummins, F.: Learning to forget: continual prediction with LSTM, Neural Comput, 12, 2451–71, 2000.

Green, J. K., Berry, J., Ciais, P., Zhang, Y., and Gentine, P.: Amazon rainforest photosynthesis increases in response to atmospheric dryness, Science Advances, 6, eabb7232, 2020.

Gu, L., Chen, J., Yin, J., Sullivan, S. C., Wang, H.-M., Guo, S., Zhang, L., and Kim, J.-S.: Projected increases in magnitude and socioeconomic exposure of global droughts in 1.5 and 2 °C warmer climates, Hydrology and Earth System Sciences, 24, 451–472, https://doi.org/10.5194/hess-24-451-2020, 2020a.

Gu, L., Chen, J., Yin, J., Xu, C.-Y., and Zhou, J.: Responses of precipitation and runoff to climate warming and implications for future drought changes in China, Earth's Future, 8, e2020EF001718, 2020b.

Gu, L., Yin, J., Zhang, H., Wang, H.-M., Yang, G., and Wu, X.: On future flood magnitudes and estimation uncertainty across 151 catchments in mainland China, International Journal of Climatology, 41, E779–E800, 2021.

Gu, L., Yin, J., Wang, S., Chen, J., Qin, H., Yan, X., He, S., and Zhao, T.: How well do the multi-satellite and atmospheric reanalysis products perform in hydrological modelling, Journal of Hydrology, 617, 128920, https://doi.org/10.1016/j.jhydrol.2022.128920, 2023.

He, B., Lü, A., Wu, J., Zhao, L., and Liu, M.: Drought hazard assessment and spatial characteristics analysis in China, Journal of Geographical Sciences, 21, 235–249, 2011.

Hu, C., Guo, S., Xiong, L., and Peng, D.: A modified Xinanjiang model and its application in northern China, Hydrology Research, 36, 175–192, 2005.

Jiang, T., Chen, Y. D., Xu, C., Chen, X., Chen, X., and Singh, V. P.: Comparison of hydrological impacts of climate change simulated by six hydrological models in the Dongjiang Basin, South China, Journal of Hydrology, 336, 316–333, https://doi.org/10.1016/j.jhydrol.2007.01.010, 2007.

Jiang, T., Jing, Z., Cheng, J., Lige, C., Yanjun, W., Hemin, S., Anqian, W., Jinlong, H., Buda, S., and Run, W.: National and provincial population projected to 2100 under the shared socioeconomic pathways in China, Advances in Climate Change Research, 13, 128, 2017.

Jiang, T., Jing, Z., Li-Ge, C. A. O., Yan-Jun, W., Bu-Da, S. U., Cheng, J., Run, W., and Chao, G. A. O.: Projection of national and provincial economy under the shared socioeconomic pathways in China, Advances in Climate Change Research, 14, 50, 2018.

Kim, J. H., Sung, J. H., Chung, E.-S., Kim, S. U., Son, M., and Shiru, M. S.: Comparison of Projection in Meteorological and Hydrological Droughts in the Cheongmicheon Watershed for RCP4. 5 and SSP2-4.5, Sustainability, 13, 2066, 2021.

Koutsoyiannis, D.: Clausius–Clapeyron equation and saturation vapour pressure: simple theory reconciled with practice, European Journal of physics, 33, 295, 2012.

Kriauciuniene, J., Jakimavicius, D., Sarauskiene, D., and Kaliatka, T.: Estimation of uncertainty sources in the projections of Lithuanian river runoff, Stochastic Environmental Research and Risk Assessment, 27, 769–784, 2013.

Kumar, R., Musuuza, J. L., Van Loon, A. F., Teuling, A. J., Barthel, R., Ten Broek, J., Mai, J., Samaniego, L., and Attinger, S.: Multiscale evaluation of the Standardized Precipitation Index as a groundwater drought indicator, Hydrology and Earth System Sciences, 20, 1117–1131, 2016.

Kundzewicz, Z., Su, B., Wang, Y., Xia, J., Huang, J., and Jiang, T.: Flood risk and its reduction in China, Advances in Water Resources, 130, 37–45, https://doi.org/10.1016/j.advwatres.2019.05.020, 2019.

Kunnath-Poovakka, A. and Eldho, T. I.: A comparative study of conceptual rainfall-runoff models GR4J, AWBM and Sacramento at catchments in the upper Godavari river basin, India, J Earth Syst Sci, 128, 33, https://doi.org/10.1007/s12040-018-1055-8, 2019.

Lange, S.: Trend-preserving bias adjustment and statistical downscaling with ISIMIP3BASD (v1.0), Geoscientific Model Development, 12, 3055–3070, https://doi.org/10.5194/gmd-12-3055-2019, 2019.

Li, D. X.: On default correlation: A copula function approach, Available at SSRN 187289, https://doi.org/10.2139/ssrn.187289, 1999.

Liu, J., Zhang, Q., Singh, V. P., and Shi, P.: Contribution of multiple climatic variables and human activities to streamflow changes across China, Journal of Hydrology, 545, 145–162, https://doi.org/10.1016/j.jhydrol.2016.12.016, 2017.

Liu, Y., Hu, Z.-Z., Wu, R., and Yuan, X.: Causes and predictability of the 2021 spring southwestern China severe drought, Advances in Atmospheric Sciences, 39, 1766–1776, 2022a.

Liu, Z., Deng, Z., He, G., Wang, H., Zhang, X., Lin, J., Qi, Y., and Liang, X.: Challenges and opportunities for carbon neutrality in China, Nat Rev Earth Environ, 3, 141–155, https://doi.org/10.1038/s43017-021-00244-x, 2022b.

Lu, R., Xu, K., Chen, R., Chen, W., Li, F., and Lv, C.: Heat waves in summer 2022 and increasing concern regarding heat waves in general, Atmospheric and Oceanic Science Letters, 16, 100290, https://doi.org/10.1016/j.aosl.2022.100290, 2023.

Ma, N., Szilagyi, J., Zhang, Y., and Liu, W.: Complementary-Relationship-Based Modeling of Terrestrial Evapotranspiration Across China During 1982–2012: Validations and Spatiotemporal Analyses, Journal of Geophysical Research: Atmospheres, 124, 4326–4351, https://doi.org/10.1029/2018JD029850, 2019.

Mallapaty, S.: China's extreme weather challenges scientists studying it, Nature, 609, 888, 2022.

Martel, J., Demeester, K., Brissette, F., Poulin, A., and Arsenault, R.: HMETS-A simple and efficient hydrology model for teaching hydrological modelling, flow forecasting and climate change impacts, International Journal of Engineering Education, 2017.

Meinshausen, M., Nicholls, Z. R., Lewis, J., Gidden, M. J., Vogel, E., Freund, M., Beyerle, U., Gessner, C., Nauels, A., and Bauer, N.: The shared socio-economic pathway (SSP) greenhouse gas concentrations and their extensions to 2500, Geoscientific Model Development, 13, 3571–3605, 2020.

Mokhtar, A., Jalali, M., He, H., Al-Ansari, N., Elbeltagi, A., Alsafadi, K., Abdo, H. G., Sammen, S. S., Gyasi-Agyei, Y., and Rodrigo-Comino, J.: Estimation of SPEI meteorological drought using machine learning algorithms, IEEE Access, 9, 65503–65523, 2021.

Myronidis, D., Ioannou, K., Fotakis, D., and Dörflinger, G.: Streamflow and hydrological drought trend analysis and forecasting in Cyprus, Water resources management, 32, 1759–1776, 2018.

Nabaei, S., Sharafati, A., Yaseen, Z. M., and Shahid, S.: Copula based assessment of meteorological drought characteristics: regional investigation of Iran, Agricultural and Forest Meteorology, 276, 107611, 2019.

Nie, N., Zhang, W., Chen, H., and Guo, H.: A global hydrological drought index dataset based on gravity recovery and climate experiment (GRACE) data, Water Resources Management, 32, 1275–1290,

2018.
O'Neill, B. C., Tebaldi, C., Van Vuuren, D. P., Eyring, V., Friedlingstein, P., Hurtt, G., Knutti, R., Kriegler, E., Lamarque, J.-F., and Lowe, J.: The scenario model intercomparison project (ScenarioMIP) for CMIP6, Geoscientific Model Development, 9, 3461–3482, 2016.
Oudin, L., Hervieu, F., Michel, C., Perrin, C., Andréassian, V., Anctil, F., and Loumagne, C.: Which potential evapotranspiration input for a lumped rainfall–runoff model?: Part 2—Towards a simple and efficient potential evapotranspiration model for rainfall–runoff modelling, Journal of Hydrology, 303, 290–306, 2005.
Pelosi, A., Terribile, F., D'Urso, G., and Chirico, G. B.: Comparison of ERA5-Land and UERRA MESCAN-SURFEX reanalysis data with spatially interpolated weather observations for the regional assessment of reference evapotranspiration, Water, 12, 1669, 2020.
Perrin, C., Michel, C., and Andréassian, V.: Improvement of a parsimonious model for streamflow simulation, Journal of hydrology, 279, 275–289, 2003.
Piao, S., Ciais, P., Huang, Y., Shen, Z., Peng, S., Li, J., Zhou, L., Liu, H., Ma, Y., Ding, Y., Friedlingstein, P., Liu, C., Tan, K., Yu, Y., Zhang, T., and Fang, J.: The impacts of climate change on water resources and agriculture in China, Nature, 467, 43–51, https://doi.org/10.1038/nature09364, 2010.
Pokhrel, Y., Felfelani, F., Satoh, Y., Boulange, J., Burek, P., Gädeke, A., Gerten, D., Gosling, S. N., Grillakis, M., and Gudmundsson, L.: Global terrestrial water storage and drought severity under climate change, Nature Climate Change, 11, 226–233, 2021.
Porter, J. W. and McMahon, T. A.: Application of a catchment model in southeastern Australia, Journal of Hydrology, 24, 121–134, 1975.
Pörtner, H.-O., Roberts, D. C., Poloczanska, E. S., Mintenbeck, K., Tignor, M., Alegría, A., Craig, M., Langsdorf, S., Löschke, S., and Möller, V.: IPCC, 2022: Summary for policymakers, 2022.
Qi, W., Chen, J., Li, L., Xu, C., Li, J., Xiang, Y., and Zhang, S.: A framework to regionalize conceptual model parameters for global hydrological modeling, Hydrology and Earth System Sciences Discussions, 1–28, https://doi.org/10.5194/hess-2020-127, 2020.
Rahmati, O., Falah, F., Dayal, K. S., Deo, R. C., Mohammadi, F., Biggs, T., Moghaddam, D. D., Naghibi, S. A., and Bui, D. T.: Machine learning approaches for spatial modeling of agricultural droughts in the south-east region of Queensland Australia, Science of the Total Environment, 699, 134230, 2020.
Ren-Jun, Z.: The Xinanjiang model applied in China, Journal of hydrology, 135, 371–381, 1992.
Schmidt, R., Schwintzer, P., Flechtner, F., Reigber, C., Güntner, A., Döll, P., Ramillien, G., Cazenave, A., Petrovic, S., and Jochmann, H.: GRACE observations of changes in continental water storage, Global and Planetary Change, 50, 112–126, 2006.
Sherstinsky, A.: Fundamentals of recurrent neural network (RNN) and long short-term memory (LSTM) network, Physica D: Nonlinear Phenomena, 404, 132306, 2020.
Shin, M.-J. and Kim, C.-S.: Component combination test to investigate improvement of the IHACRES and GR4J rainfall–runoff models, Water, 13, 2126, 2021.
Shukla, S. and Wood, A. W.: Use of a standardized runoff index for characterizing hydrologic drought, Geophysical research letters, 35, 2008.
Simmons, A. J., Untch, A., Jakob, C., Kållberg, P., and Undén, P.: Stratospheric water vapour and tropical tropopause temperatures in Ecmwf analyses and multi-year simulations, , 125, 353–386, 1999.
Sohn, J. A., Saha, S., and Bauhus, J.: Potential of forest thinning to mitigate drought stress: A meta-analysis, Forest Ecology and Management, 380, 261–273, https://doi.org/10.1016/j.foreco.2016.07.046, 2016.
Sönmez, A. Y. and Kale, S.: Climate change effects on annual streamflow of Filyos River (Turkey), Journal of Water and Climate Change, 11, 420–433, https://doi.org/10.2166/wcc.2018.060, 2018.
Stewart, I. T.: Changes in snowpack and snowmelt runoff for key mountain regions, Hydrological Processes, 23, 78–94, https://doi.org/10.1002/hyp.7128, 2009.
Tabari, H.: Climate change impact on flood and extreme precipitation increases with water availability, Scientific reports, 10, 1–10, 2020.
Tapley, B. D., Bettadpur, S., Ries, J. C., Thompson, P. F., and Watkins, M. M.: GRACE measurements of mass variability in the Earth system, science, 305, 503–505, 2004.
Tian, Y., Xu, Y.-P., and Zhang, X.-J.: Assessment of Climate Change Impacts on River High Flows through Comparative Use of GR4J, HBV and Xinanjiang Models, Water Resources Management, 27, 2871–2888, 2013.

Tirivarombo, S., Osupile, D., and Eliasson, P.: Drought monitoring and analysis: standardised precipitation evapotranspiration index (SPEI) and standardised precipitation index (SPI), Physics and Chemistry of the Earth, Parts A/B/C, 106, 1–10, 2018.
Udall, B. and Overpeck, J.: The twenty-first century Colorado River hot drought and implications for the future, Water Resources Research, 53, 2404–2418, 2017.
Vicente-Serrano, S. M., López-Moreno, J. I., Beguería, S., Lorenzo-Lacruz, J., Azorin-Molina, C., and Morán-Tejeda, E.: Accurate computation of a streamflow drought index, Journal of Hydrologic Engineering, 17, 318–332, 2012.
Wang, Z., Li, J., Lai, C., Zeng, Z., Zhong, R., Chen, X., Zhou, X., and Wang, M.: Does drought in China show a significant decreasing trend from 1961 to 2009?, Science of The Total Environment, 579, 314–324, https://doi.org/10.1016/j.scitotenv.2016.11.098, 2017.
Weinfurt, K. P.: Multivariate analysis of variance, in: Reading and understanding multivariate statistics, American Psychological Association, Washington, DC, US, 245–276, 1995.
Wilhite, D. A., Svoboda, M. D., and Hayes, M. J.: Understanding the complex impacts of drought: A key to enhancing drought mitigation and preparedness, Water Resour Manage, 21, 763–774, https://doi.org/10.1007/s11269-006-9076-5, 2007.
Woolway, R. I., Kraemer, B. M., Lenters, J. D., Merchant, C. J., O'Reilly, C. M., and Sharma, S.: Global lake responses to climate change, Nat Rev Earth Environ, 1, 388–403, https://doi.org/10.1038/s43017-020-0067-5, 2020.
Wu, J., Chen, X., Yao, H., and Zhang, D.: Multi-timescale assessment of propagation thresholds from meteorological to hydrological drought, Science of the Total Environment, 765, 144232, 2021.
Wu, X., Guo, S., Yin, J., Yang, G., Zhong, Y., and Liu, D.: On the event-based extreme precipitation across China: Time distribution patterns, trends, and return levels, Journal of hydrology, 562, 305–317, 2018.
Xiao-jun, W., Jian-yun, Z., Shahid, S., ElMahdi, A., Rui-min, H., Zhen-xin, B., and Ali, M.: Water resources management strategy for adaptation to droughts in China, Mitig Adapt Strateg Glob Change, 17, 923–937, https://doi.org/10.1007/s11027-011-9352-4, 2012.
Xiujia, C., Guanghua, Y., Jian, G., Ningning, M., and Zihao, W.: Application of WNN-PSO model in drought prediction at crop growth stages: A case study of spring maize in semi-arid regions of northern China, Computers and Electronics in Agriculture, 199, 107155, 2022.
Xu, K., Yang, D., Yang, H., Li, Z., Qin, Y., and Shen, Y.: Spatio-temporal variation of drought in China during 1961–2012: A climatic perspective, Journal of Hydrology, 526, 253–264, 2015.
Yao, F., Livneh, B., Rajagopalan, B., Wang, J., Crétaux, J.-F., Wada, Y., and Berge-Nguyen, M.: Satellites reveal widespread decline in global lake water storage, Science, 380, 743–749, https://doi.org/10.1126/science.abo2812, 2023.
Yevjevich, V. M.: Objective approach to definitions and investigations of continental hydrologic droughts, An, PhD Thesis, Colorado State University. Libraries, 1967.
Yihdego, Y., Vaheddoost, B., and Al-Weshah, R. A.: Drought indices and indicators revisited, Arab J Geosci, 12, 69, https://doi.org/10.1007/s12517-019-4237-z, 2019.
Yilmaz, M.: Accuracy assessment of temperature trends from ERA5 and ERA5-Land, Science of The Total Environment, 856, 159182, https://doi.org/10.1016/j.scitotenv.2022.159182, 2023.
Yin, J., Guo, S., He, S., Guo, J., Hong, X., and Liu, Z.: A copula-based analysis of projected climate changes to bivariate flood quantiles, Journal of hydrology, 566, 23–42, 2018.
Yin, J., Guo, S., Gu, L., He, S., Ba, H., Tian, J., Li, Q., and Chen, J.: Projected changes of bivariate flood quantiles and estimation uncertainty based on multi-model ensembles over China, Journal of Hydrology, 585, 124760, 2020.
Yin, J., Guo, S., Gu, L., Zeng, Z., Liu, D., Chen, J., Shen, Y., and Xu, C.-Y.: Blending multi-satellite, atmospheric reanalysis and gauge precipitation products to facilitate hydrological modelling, Journal of Hydrology, 593, 125878, 2021a.
Yin, J., Guo, S., Gentine, P., Sullivan, S. C., Gu, L., He, S., Chen, J., and Liu, P.: Does the hook structure constrain future flood intensification under anthropogenic climate warming?, Water Resources Research, 57, e2020WR028491, 2021b.
Yin, J., Guo, S., Yang, Y., Chen, J., Gu, L., Wang, J., He, S., Wu, B., and Xiong, J.: Projection of droughts and their socioeconomic exposures based on terrestrial water storage anomaly over China, Sci. China Earth Sci., 65, 1772–1787, https://doi.org/10.1007/s11430-021-9927-x, 2022.
Yin, J., Gentine, P., Slater, L., Gu, L., Pokhrel, Y., Hanasaki, N., Guo, S., Xiong, L., and Schlenker, W.:

Future socio-ecosystem productivity threatened by compound drought–heatwave events, Nat Sustain, 6, 259–272, https://doi.org/10.1038/s41893-022-01024-1, 2023a.
Yin, J., Guo, S., Wang, J., Chen, J., Zhang, Q., Gu, L., Yang, Y., Tian, J., Xiong, L., and Zhang, Y.: Thermodynamic driving mechanisms for the formation of global precipitation extremes and ecohydrological effects, Sci. China Earth Sci., 66, 92–110, https://doi.org/10.1007/s11430-022-9987-0, 2023b.
Yu, B. and Zhu, Z.: A comparative assessment of AWBM and SimHyd for forested watersheds, Hydrological sciences journal, 60, 1200–1212, 2015.
Yu, Y., Si, X., Hu, C., and Zhang, J.: A Review of Recurrent Neural Networks: LSTM Cells and Network Architectures, Neural Comput, 31, 1235–1270, 2019.
Zhai, P. M. and Zou, X. K.: Changes in temperature and precipitation and their impacts on drought in China during 1951–2003, Advances in Climate Change Research, 1, 16–18, 2005.
Zhang, F., Deng, X., Xie, L., and Xu, N.: China's energy-related carbon emissions projections for the shared socioeconomic pathways, Resources, Conservation and Recycling, 168, 105456, 2021.
Zhang, G., Gan, T. Y., and Su, X.: Twenty-first century drought analysis across China under climate change, Climate Dynamics, 59, 1665–1685, 2022.
Zhao, M., A, G., Velicogna, I., and Kimball, J. S.: Satellite Observations of Regional Drought Severity in the Continental United States Using GRACE-Based Terrestrial Water Storage Changes, Journal of Climate, 30, 6297–6308, https://doi.org/10.1175/JCLI-D-16-0458.1, 2017.
Zheng, J., Wang, H., and Liu, B.: Impact of the long-term precipitation and land use changes on runoff variations in a humid subtropical river basin of China, Journal of Hydrology: Regional Studies, 42, 101136, 2022.
Zhu, Q., Luo, Y., Zhou, D., Xu, Y.-P., Wang, G., and Tian, Y.: Drought prediction using in situ and remote sensing products with SVM over the Xiang River Basin, China, Natural Hazards, 105, 2161–2185, 2021.